AD-A094 010 IOWA UNIV IOWA CITY DEPT OF PHYSICS AND ASTRONOMY F/G 4/1
PLASMA WAVES ASSOCIATED WITH ENERGETIC PARTICLES STREAMING INTO--ETC(U)
DEC 80 R R ANDERSON, G K PARKS, T E EASTMAN N00014-76-C-0016
UNCLASSIFIED U OF IOWA-80-40 NL

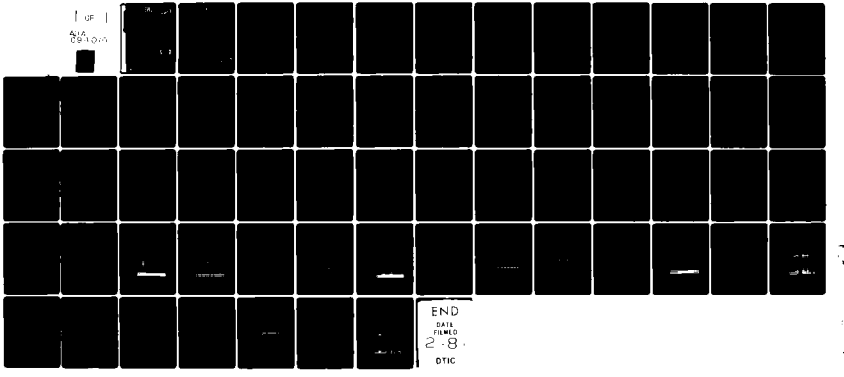

LEVEL II

U. of Iowa 80-40

12

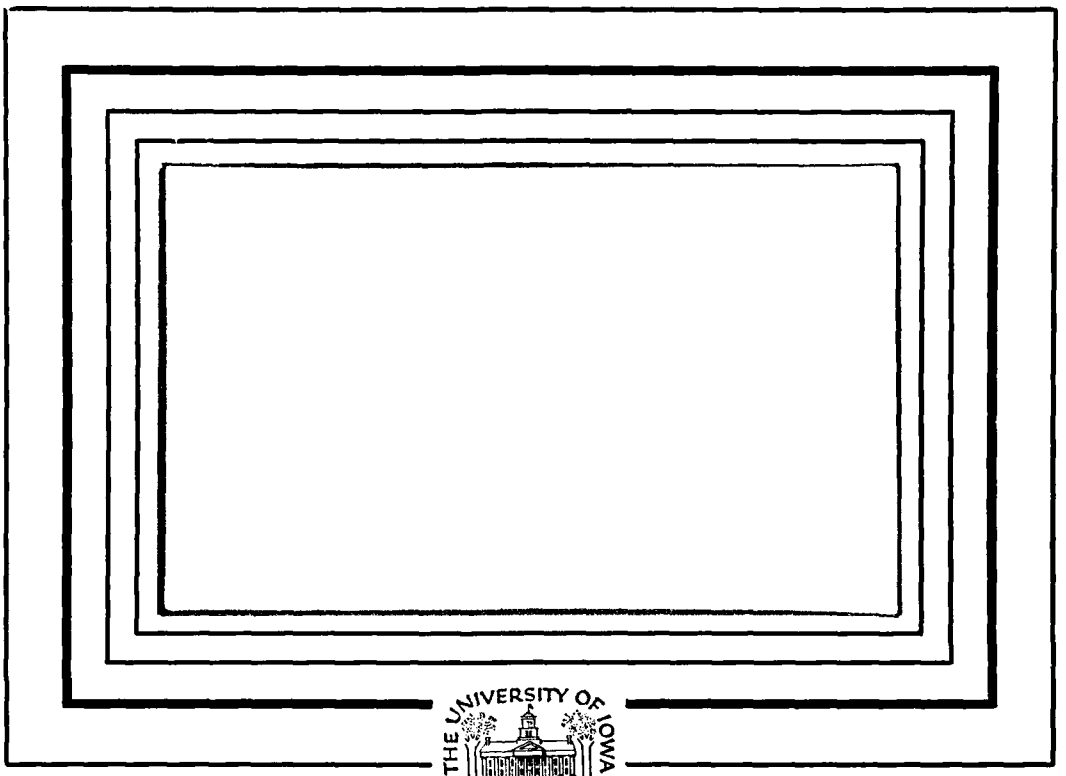

Department of Physics and Astronomy

THE UNIVERSITY OF IOWA

Iowa City, Iowa 52242

81 1 21 030

LEVEL II

12

U. of Iowa 80-40

Plasma Waves Associated With Energetic Particles Streaming into the Solar Wind from the Earth's Bow Shock

by

R. R. Anderson, G. K. Parks*, T. E. Eastman,
D. A. Gurnett, and L. A. Frank

July, 1980

Department of Physics and Astronomy
The University of Iowa
Iowa City, IA 52242

*Geophysics Program
University of Washington
Seattle, WA 98195

UNCLASSIFIED

SECURITY CLASSIFICATION OF THIS PAGE (When Data Entered)

REPORT DOCUMENTATION PAGE

READ INSTRUCTIONS BEFORE COMPLETING FORM

1. REPORT NUMBER: U. of Iowa 80- -6	2. GOVT ACCESSION NO.: AD-A094 010
3. RECIPIENT'S CATALOG NUMBER:	
4. TITLE (and Subtitle): PLASMA WAVES ASSOCIATED WITH ENERGETIC PARTICLES STREAMING INTO THE SOLAR WIND FROM THE EARTH'S BOW SHOCK.	5. TYPE OF REPORT & PERIOD COVERED: Progress July 1980
	6. PERFORMING ORG. REPORT NUMBER:
7. AUTHOR(s): R. R. ANDERSON, G. K. PARKS, T. E. EASTMAN, D. A. GURNETT AND L. A. FRANK	8. CONTRACT OR GRANT NUMBER(s): N00014-76-C-0016
9. PERFORMING ORGANIZATION NAME AND ADDRESS: Department of Physics and Astronomy, The University of Iowa, Iowa City, IA 52242	10. PROGRAM ELEMENT, PROJECT, TASK AREA & WORK UNIT NUMBERS:
11. CONTROLLING OFFICE NAME AND ADDRESS: Office of Naval Research, Electronics Program Office, Arlington, VA 22217	12. REPORT DATE: 8 December 1980
	13. NUMBER OF PAGES: 59
14. MONITORING AGENCY NAME & ADDRESS(if different from Controlling Office): 14 U OF	15. SECURITY CLASS. (of this report): UNCLASSIFIED
	15a. DECLASSIFICATION/DOWNGRADING SCHEDULE:

16. DISTRIBUTION STATEMENT (of this Report)

Approved for public release; distribution is unlimited

17. DISTRIBUTION STATEMENT (of the abstract entered in Block 20, if different from Report)

18. SUPPLEMENTARY NOTES

To be published in J. Geophys. Res.

19. KEY WORDS (Continue on reverse side if necessary and identify by block number)

Particles and fields
Interplanetary space

20. ABSTRACT (Continue on reverse side if necessary and identify by block number)

(See following page)

DD FORM 1 JAN 73 1473 EDITION OF 1 NOV 65 IS OBSOLETE
S/N 0102-014-6601

UNCLASSIFIED
SECURITY CLASSIFICATION OF THIS PAGE (When Data Entered)

ABSTRACT

In the upstream solar wind, three dominant types of plasma waves are observed associated with energetic particle streams coming from the earth's bow shock: ion-acoustic waves, electron plasma oscillations, and whistler-mode waves. The ion-acoustic waves occur simultaneously with either ion beams or a dispersed ion population in the energy range from ~ 0.5 to > 45 keV. These short-wavelength electrostatic waves are very impulsive and the peak amplitudes increase with increasing ion flux and at spatial gradients in the energetic ion densities. The electron plasma oscillations are long-wavelength nearly monochromatic electrostatic waves which are closely correlated with the flux of low energy electrons, especially in the 0.2 - 1.5 keV range. In the presence of only enhanced electron fluxes, the average amplitudes of the electron plasma oscillations approach the peak amplitudes. Amplitudes near 10 mV/m have been observed, although amplitudes from 0.1 to 1.0 mV/m are typical. In the presence of the dispersed ion component, electron plasma oscillations decrease in amplitude and become more impulsive. Electromagnetic waves with frequencies below 200 Hz are observed when either ion beams or dispersed ion distributions are present. These waves are usually weak and very impulsive. For these waves the refractive index determined from the wave B to E ratio is consistent with whistler-mode radiation. Whistler-mode waves also occasionally occur in association with electron plasma oscillations.

I. INTRODUCTION

The purpose of this paper is to describe and interpret the electrostatic and electromagnetic plasma waves observed on ISEE 1 and 2 in the region upstream of the earth's bow shock and their association with upstream energetic plasma. This paper will emphasize the characteristics of the plasma waves. Companion papers by Eastman et al. [1980] and Parks et al. [1980] will emphasize the characteristics of the plasma associated with these waves in the upstream solar wind. The major significance of the research that we report here is that we are able to evaluate the wave-particle interactions in detail to a degree not possible in previous investigations. The data we use are from two ISEE spacecraft which are similarly instrumented and travel together in nearly identical orbits. The electric antennas on the two spacecraft have a significant difference in length such that the range of wavelength values can be investigated. High-time resolution measurements, as fast as 32 samples per second, are used both for wave amplitudes over the frequency range from 5.6 Hz to 311 kHz and for the fluxes of ions and electrons over the energy range from ~ 1 keV to > 290 keV. On these time scales we are able to observe directly the rapid changes that occur when the waves and particles interact.

The three dominant types of plasma waves associated with particles in the upstream solar wind are ion-acoustic waves, electron plasma oscillations and whistler-mode waves. The waves identified as

ion-acoustic waves are electrostatic waves which occur simultaneously with either ion beams or dispersed ion distributions in the energy range from ~ 0.5 to > 45 keV. The first observation of high frequency (f ~ 2 to 5 kHz) electrostatic waves associated with upstream 4 to 7 keV proton fluxes was made by Scarf et al. [1970]. They found that intense electrostatic noise bursts were produced when steep gradients in the magnetic field were encountered. Doppler-shifted ion-acoustic waves, Buneman-mode waves, and other slow modes associated with the ion plasma frequency were suggested as likely candidates for these waves. Wave spectra comparisons between measurements taken from ISEE 1 and 2, which have different electric antenna lengths, show that the wavelengths are typically between 30 and 215 meters. The spectra of these short-wavelength electrostatic waves have a broad peak covering the frequency range from a few hundred Hz to many kHz primarily due to Doppler shifts resulting from the solar wind flow. From similar observations on IMP 6 of these high frequency electrostatic waves associated with upstream protons, Gurnett and Frank [1978] concluded that the waves were short-wavelength Doppler-shifted ion-acoustic waves.

Electron plasma oscillations are long-wavelength electrostatic waves occurring near the local electron plasma frequency. These waves were first observed upstream of the bow shock by Fredricks et al. [1968]. Scarf et al. [1971] found that waves near the electron plasma frequency were produced by suprathermal electrons ($E_e \gtrsim 700$ to 800 eV) flowing upstream of the bow shock. Based on our analysis of the ISEE data, we find that the occurrence and the amplitudes of electron plasma oscillations are closely correlated with the flux of low energy

electrons, especially in the 0.2 to 1.5 keV range. The onset of electron plasma oscillations and the abrupt increase in the flux of low energy electrons occur simultaneously down to time scales on the order of seconds. During intense electron plasma oscillation events, weak low-frequency electrostatic waves are also observed. Whistler-mode waves also occasionally occur with electron plasma oscillations. This association was first observed with ISEE 3 far upstream of the bow shock by Kennel et al. [1980].

Electromagnetic waves with frequencies below 200 Hz are observed when either ion beams or the dispersed ion distributions are present. For these waves the refractive index determined from the wave B to E ratio is consistent with whistler-mode radiation.

II. SPACECRAFT AND EXPERIMENT DESCRIPTIONS

ISEE 1 and 2 were launched on October 22, 1977, into nearly identical eccentric Earth orbits having a 22.5 R_E apogee geocentric distance, an orbital period of 57.3 hours, and an inclination of about 30° to the ecliptic plane. The local time of apogee at launch was about ten hours and it decreases at a rate of 2 hours per month. This trajectory took ISEE 1 and 2 through the bow shock and into the upstream solar wind nearly every orbit for the first several months of operation. This provided excellent opportunities for studying the upstream solar wind and the wave particle interactions taking place there under a variety of magnetic field directions and solar wind conditions.

The plasma wave data used in this study came from The University of Iowa Plasma Wave Experiments on ISEE 1 and 2. Complete descriptions of these experiments are given in Gurnett et al. [1978]. Here we will review the instrumentation pertinent to this study. For ISEE 1, the electric sensor is a 215 meter electric dipole antenna. The magnetic sensor is a search coil magnetic antenna. ISEE 1 has a 20-channel electric spectrum analyzer covering the frequency range from 5.6 Hz to 311 kHz and a 14-channel magnetic spectrum analyzer covering the frequency range from 5.6 Hz to 10 kHz. ISEE 1 also has a 128 channel sweep frequency receiver covering the frequency range from 100 Hz to 400 kHz and a wideband receiver with selectable 10 kHz and 40 kHz bandwidths and eight commandable base frequencies from 0 Hz to 2 MHz.

For ISEE 2, the electric sensor is a 30 meter electric dipole antenna. A single 16 channel spectrum analyzer on ISEE 2 covers the frequency range from 5.6 Hz to 31.1 kHz. The ISEE 2 wideband receiver is identical to that on ISEE 1 except that it has only the 10 kHz bandwidth.

The plasma measurements used in this study are obtained from The University of Iowa quadrispherical plasma analyzers (LEPEDEAs) on ISEE 1 and 2. Detailed descriptions of these instruments are given in Frank et al. [1978a, 1978b]. These LEPEDEAs are capable of measuring an E/Q range of 1 eV to 45 keV in 64 contiguous passbands for positive ions and electrons. Seven pairs of sensors segment a total field of view of 6 x 162° into seven contiguous fields-of-view oriented along the spacecraft spin axis. The ion and electron sensors are sampled 12 or 16 times per spacecraft spin to fill in a three-dimensional velocity distribution that covers all except ~ 2% of the unit sphere for particle velocity vectors. Instrument cycle times for the LEPEDEAs are two minutes and eight minutes for the high-bit-rate and low-bit-rate modes, respectively.

The energetic particle measurements used in this study are obtained on both ISEE 1 and 2 from instruments developed by the University of California, Berkeley; Paul Sabatier University, Toulouse, France; and the University of Washington. Detailed descriptions of this instrumentation are given in Anderson et al. [1978] and Parks et al. [1978]. These instruments use fixed voltage electrostatic analyzers and semiconductor detector telescopes and span the energy range from ~ 1.3 keV to ~ 290 keV for both electrons and protons. The view direction of the detectors is along the spacecraft spin axis which is nearly perpendicular to the ecliptic plane.

III. ION-ACOUSTIC WAVES

In the region upstream from the earth's bow shock, the predominant electrostatic plasma waves associated with enhanced ion flux events are ion-acoustic waves. A classic example of this association occurs in the time period from 2000 to 2100 UT on day 312, November 8, 1977, and is illustrated in Figures 1 and 2. On November 8 the ISEE spacecraft crossed the bow shock and entered the upstream region about 1850 UT at a radial distance of 15.7 R_E and a magnetic local time (MLT) of 8.3 hours. A little over one hour later, at a radial distance of about 17 R_E, the spacecraft encountered large and abrupt increases in ion fluxes accompanied by large and abrupt enhancements in ion-acoustic wave amplitudes. Examination of the magnetic field parameters from the data pool tape shows that this event occurred when the magnetic field changed in such a way that the ISEE spacecraft were brought into the ion foreshock region. The lower panels of Figures 1 and 2 show the electric spectrum analyzer data for ISEE 2 and 1, respectively. The top line plotted for each channel represents the peak amplitude measured over 6 second time intervals and the shaded area represents average amplitudes over the same time intervals. Full scale for each channel equals 100 dB in amplitude. The top panel of Figure 1 shows the fluxes of ions in the energy ranges 1.3 to 1.7 keV, 5.4 to 6.6 keV and 19 to 290 keV measured on ISEE 2 viewing along the spacecraft spin axis. The top panel of Figure 2 shows the fluxes of electrons in the energy ranges 1.4 to 1.6 keV and 4.5 to 6.0 keV measured on ISEE 2 also viewing along the spacecraft spin axis.

Coincident with the change in the magnetic field direction at 2005 UT, the ion fluxes abruptly increase and begin to fluctuate rapidly. The fluxes of 1.3 to 1.7 keV and 5.4 to 6.6 keV ions suddenly increase by 2 1/2 orders of magnitude to about 10^6 and 10^5 $(cm^2$ sec ster keV$)^{-1}$, respectively. The 19-290 keV ion fluxes increase more than an order of magnitude to about 5×10^4 $(cm^2$ sec ster keV$)^{-1}$. The flux increases are very abrupt and continue to fluctuate one to two orders of magnitude throughout the event until about 2034 when the high fluxes terminate as abruptly as they began. The termination of this event is coincident with a return of the magnetic field direction to near the direction it had before the event started. The upstream particle flux events typically have extremely sharp onsets and recoveries. Particle fluxes can change by more than an order of magnitude in less than a second. Ion velocity distributions determined by the quadrispherical LEPEDEA instrument on ISEE 1 show that the enhanced ion flux event at this time consists of a "diffuse" or dispersed ion distribution and that the flux enhancement extends down in energy to about 0.5 keV in the spacecraft frame of reference.

The most notable feature in the plasma wave data associated with this enhanced ion flux event is an abrupt increase in electrostatic waves from 2003 to 2035 UT which we identify as Doppler-shifted ion-acoustic waves. In the ISEE 2 data they are evident from about 178 Hz to 10 kHz and in the ISEE 1 data they are evident from 100 Hz to 5.6 kHz. The waves are very impulsive with peak amplitudes typically one to two orders of magnitude greater than the average amplitude. The electrostatic nature of the waves is verified by the fact that no signals above 178 Hz are present in the ISEE 1 magnetic spectrum analyzer data during the event. A comparison of the ion-acoustic wave spectral

densities between ISEE 1 and 2 is shown in Figure 3 where the data have been accumulated over the time interval from 2011 to 2012 UT. The ISEE 1 spectral density peaks at 1.8 kHz while the ISEE 2 spectral density peaks between 1.8 kHz and 3.1 kHz. Above 311 Hz, the ion-acoustic wave spectral densities on ISEE 2, the spacecraft with the shorter antenna, exceed those on ISEE 1. The reduction of the field strength on the longer antenna identifies the wavelength of the ion-acoustic waves as being between 30 meters and 215 meters, the lengths of the two antennas. The peak amplitude of the ion-acoustic waves integrated over frequency for this event was 6 mV/m.

High-resolution frequency-time spectrograms of the ion-acoustic waves observed on ISEE 2 during the ion enhancement event are shown in Figure 4. While the signals are usually most intense below 2 kHz, frequently they rise to near 9 kHz in fractions of a second. The emissions are quite narrowband with instantaneous bandwidths ranging from a few hundred Hz to about 1 kHz. The large bandwidth structure of the emissions observed in the spectrograms is due to the rapidly varying center frequency. Both rapidly rising and rapidly falling bands are observed. Commonly observed features are hook-like bands that fall in frequency for about a second and then rise in frequency for another second.

Identification of these waves as Doppler-shifted ion-acoustic waves is based on the following analysis. Ion-acoustic waves have frequencies $f \lesssim fp_i$, the ion plasma frequency, and a phase speed $V_p = \frac{\omega}{k} \simeq c_s$, the ion sound speed. For the time period covered in Figures 3 and 4, 2011 to 2020 UT, the electron number density, N_e, varies from 9 to 26 cm^{-3} and averages about 16 cm^{-3} [Paschmann et al., 1979, Figure 3]. The electron temperature is about 1.4×10^5 °K [Jack Scudder, private communication]. For these conditions, $c_s \simeq 34$ km/sec, fp_i (assuming

protons are the dominate ions) ranges from 630 Hz to 1.1 kHz and averages 840 Hz and λ_D, the debye length ranges from 5.1 m to 8.6 m and averages 6.5 m. The minimum wavelength calculated $\lambda_{min} = 2\pi\lambda_D$, is 41 m. For f = 178 Hz $\simeq .2\ f_{pi}$, $\lambda \sim 190$ m for $V_p = c_s$. These extremes in wavelength are in good agreement with our wavelength observations. The Doppler shift, Δf, observed in the spacecraft frame of reference is

$$\Delta f \simeq (V_{sw}/\lambda)\mathrm{Cos}\theta_{kV}$$

where θ_{kV} is the angle between the propagation vector and the solar wind velocity. The solar wind speed as given by the ISEE data pool tape is $V_{sw} \simeq 450$ km/sec. The maximum possible Doppler shift is $V_{sw}/\lambda_{min} \simeq 11$ kHz. The highest frequencies we observe are just below this limit. The rapidly varying center frequencies can be accounted for both by rapid changes in θ_{kV} due to the magnetic field changing direction and changes in the wavelengths of the waves.

The ISEE 1 spectrograms (not shown) corresponding to Figure 4 are nearly identical to the ISEE 2 spectrograms except that the features in the two spectrograms are offset by about one second. Examination of the ion flux graphs for the two spacecraft indicates the same offset. This offset represents the time for the ions and the waves to convect downstream past one spacecraft and then the other. The same offset time for both the ion fluxes and the ion-acoustic wave emissions indicates that the ion-acoustic wave are generated locally by some process involving the ions.

Of interest to note in Figure 2 is the change in the low energy electron flux and in the electron plasma oscillations that occurs coincident with the enhanced proton flux event. The 1.4 to 1.6 keV electron

flux fluctuates about a half an order of magnitude during the event and the electron plasma oscillations are very sporadic and impulsive and typically much less intense than those observed in the absence of enhanced ion fluxes. In general, when upstream ion fluxes are detected, there is a tendency for the electron fluxes to be slightly increased. Later we will see that low energy electron fluxes can be enhanced without any accompanying enhancement of the low energy ion fluxes. Whether electrons and ions are detected simultaneously or not depends on the relative position of the spacecraft, the bow shock and the geometry of the interplanetary magnetic field [Anderson et al., 1979; Eastman et al., 1980]. The presence of electrons in the absence of ions usually occurs when the spacecraft is downstream from the electron foreshock boundary but upstream of the ion foreshock boundary.

Two well-defined upstream ion events occur in the following hour as shown in Figure 5. The top panel shows that a moderately intense ion flux enhancement occurs from about 2112 to 2124 UT. The upstream ion fluxes are enhanced over a broad energy range, from 1.3 keV to $\gtrsim$ 19 keV. Peak flux for the 1.3 to 1.7 keV protons at a pitch angle of $\sim 80°$ is about 5×10^5 $(cm^2 \text{ sec ster keV})^{-1}$ during the enhancement which is about 2 1/2 orders of magnitude above the pre-enhancement level. The lower panel, which contains the ISEE 2 plasma wave data, shows that the ion flux enhancement is associated with impulsive ion-acoustic waves covering the frequency range from 178 Hz to 10 kHz. Similar to the first event discussed, this ion flux enhancement event occurred when the magnetic field changed in such a way as to bring the ISEE spacecraft into the ion foreshock region.

An expanded display of the first ion flux enhancement event is shown in Figure 6. The fluxes of ions with energies of 1.3 to 1.7 keV and 5.4 to 6.6 keV are displayed simultaneously with the ISEE 1 electric field wave data from 5.6 Hz to 56 kHz. On this time scale we see that the particle fluxes occur in bursts with durations of a few seconds to about one minute. Wave-particle correlations on this time scale are clearly present although very complex. The wave bursts often appear narrower than the particle bursts and they appear both near rapid changes in the particle flux and near ion flux peaks. Parks et al. [1980] show that most of the rapid changes in the particle fluxes represent particle spatial gradients.

From 2132 to 2136 UT an even more intense ion flux enhancement event occurs. The peak flux for the 1.3 to 1.7 keV ions exceeds 10^6 $(cm^2\ sec\ ster\ keV)^{-1}$. As shown in Figure 5, the ion-acoustic wave amplitudes are greater during the more intense ion flux enhancement event than during the earlier somewhat weaker event. The plasma waves also extend to lower frequencies than during the earlier event. An E-ϕ spectrogram for this time period (Plate 4 of Eastman et al. [1980]) shows that the ion distribution is of the dispersed type.

The top panel of Figure 7 shows the low energy electron flux observed from 2100 to 2200 UT on November 8. From the onset of the first proton flux enhancement event to the end of the second proton flux enhancement event, the 1.4 to 1.6 keV electron flux is enhanced sporadically by about one-half an order of magnitude. The 4.5 to 6.0 keV electrons show a slight enhancement only during the second, more intense proton flux enhancement. The two lower panels show the ISEE 1 electric and magnetic spectrum analyzer data. The electric field data on ISEE 1

are similar to those on ISEE 2. The ion-acoustic wave amplitudes are more intense during the more intense proton flux enhancement event. In the magnetic field data in the lower panel we see that magnetic turbulence is also associated with the ion flux enhancements. This correlation will be discussed in Section V.

Ion-acoustic waves and whistler-mode emissions have the same correlation with ion beam events as they do with the dispersed ion distributions. An ion beam is observed in the ISEE 1 Lepedea data [Eastman et al., 1980, Plate 1] with energy between 1 and 2 keV in the spacecraft frame of reference in the duskward quadrant from about 2335 to 2350 UT on November 6, 1977. In the electric spectrum analyzer data in Figure 8, ion-acoustic waves from 100 Hz to 5.6 kHz begin about 2335 and end about 2350, coincident with the ion beam. Weak and sporadic whistler-mode waves from 5.6 Hz to 56 Hz also occur coincident with the ion beam event. From studying many ion beam events we have found that similar to the dispersed ion distribution events, sporadic and impulsive ion-acoustic waves and whistler-mode waves whose intensities increase with increasing beam strength occur simultaneously with ion beam events.

Polarization measurements for ion-acoustic waves are usually difficult to make because of the impulsive character of the waves and the rapidly varying magnetic field that frequently accompanies ion flux events. When polarization measurements are possible, we usually find that peak amplitudes for the ion-acoustic waves usually occur near where the electric antenna is most nearly aligned along the ambient magnetic field direction. Two examples of polarization measurements for ion-acoustic waves are shown in Figure 9. Figure 9a shows rapid sample data for 4 seconds around 1036 UT on November 6, 1977, during a high bit

rate pass. The 3.1 kHz-channel is being sampled at 32 samples per second. The solar wind magnetic field had almost no Y component. It was pointed anti-sunward and about 15° below the ecliptic plane. The arrows indicate when the antenna is most nearly parallel to the ambient magnetic field. The peak in the ion-acoustic wave amplitude occurs when the antenna is most nearly aligned with the ambient magnetic field.

Figure 9b shows rapid sample data for 16 seconds around 2027 UT on November 8, 1977, during a low bit rate pass. The 5.6 kHz-channel is being sampled at 8 times per second. The solar wind magnetic field was in the ecliptic plane to within a few degrees. Three strong peaks occur very near where the antenna is aligned along the magnetic field. Away from this alignment, the field strengths rapidly drop one to two orders of magnitude. However, as indicated by the first peak in the plot, the field strengths sometime peak at an angle away from the magnetic field direction. It is not possible to determine whether this indicates off-angle propagation or is just caused by impulsive event lasting less than half a spin period. The majority of the time when polarization measurements are possible, we find that the ion-acoustic waves have their peak amplitudes when the electric antenna is directed most nearly parallel to the ambient magnetic field. These results are in agreement with other polarization measurements of ion-acoustic waves in the solar wind by Gurnett and Frank [1978].

Gurnett and Frank [1978] in their study of ion-acoustic waves in the solar wind suggested two possible mechanisms for the generation of ion-acoustic waves by protons streaming into the solar wind from the bow shock. They found that the instability might be caused directly by a double peak in the proton distribution or that the instability might be

caused indirectly by a shift in velocity of the core electrons required to maintain zero net current. Ion distribution functions during times when we observed ion-acoustic waves have been shown in Eastman et al. [1980, Figures 3 and 4]. Double peaks in both the ion distribution functions for an ion beam event and for a dispersed ion flux event are clearly evident but at speeds comparable to the solar wind speed. We cannot determine whether or not the positive slopes at the secondary peaks are sufficient to produce ion-acoustic waves because the corresponding electron distribution functions are below our measurement capabilities. It may be the case that the energetic ions we are observing do not directly generate the ion-acoustic waves. Because the observed beam velocities are so much larger than the ion thermal velocity, Gary [1980] argues that it is unlikely that the energetic ion beam is the source of the ion-acoustic waves. Because of the good correlation we observe between the ~ 1 keV ions and the ion-acoustic waves, it is possible that we are observing the high energy end of the distribution that directly causes the waves. This is supported by the fact that when ion-acoustic waves are observed, enhanced low energy ions are observed more frequently than the higher energy ions.

Parks et al. [1980] and Wu et al. [1980] have studied the problem of generating low frequency waves by a small population of upstream energetic protons streaming relative to the solar wind with a density gradient. They have found that waves with frequencies appropriate for ion-acoustic waves will be excited. However, the wavelengths are much longer than λ_D and the polarization of the waves is still being studied. These studies do support our observations of enhanced plasma waves at spatial gradients in energetic ion densities.

IV. ELECTRON PLASMA OSCILLATIONS

In the upstream solar wind, the predominant electrostatic plasma waves associated with enhanced electron flux events are electron plasma oscillations. An example of the association between low energy electrons and electron plasma oscillations is illustrated in Figure 10. Coincident with an abrupt increase in the flux of 1.4 to 1.6 keV electrons, we observe an abrupt onset of electron plasma oscillations primarily in the 31-kHz channel. Wideband analog and sweep frequency receiver observations indicate that the electron plasma oscillations are nearly monochromatic. The presence of signals resembling electron plasma oscillations in adjacent channels is due to the finite roll-off in the spectrum analyzer filters. The electron plasma oscillations cease abruptly when the low energy electron enhancement terminates. The electron enhancement is most pronounced in the 1.4 to 1.6 keV channel which typically varies one-half to one order of magnitude. In the 4.5 to 6.0 keV channel much weaker enhancements occur indicating a fairly steep electron spectrum. Examination of the LEPEDEA E-t spectrograms indicate that the electron enhancement extends down to $\lesssim$ 0.2 keV. Anderson et al. [1979] show that these electron enhancement events occur when the solar wind magnetic field changes in such a way to put the spacecraft in the electron foreshock region.

Figure 11, a spectral density comparison between ISEE 1 and 2, shows that the electron plasma oscillations have long wavelengths. Although the antenna lengths on ISEE 1 and 2 differ by a factor of

seven, the spectral density measurement for the electron plasma oscillations are nearly identical on the two spacecraft. This indicates that the wavelengths are substantially longer than 215 meters, the length of the longer antenna [Gurnett et al., 1979]. Gurnett and Frank [1975] estimated that the wavelength of the upstream plasma oscillations is of the order of several kilometers.

On ISEE 1 and 2 we cannot demonstrate the electrostatic character of the electron plasma oscillations unless the electron plasma frequency falls in the range of the magnetic receiver whose upper frequency cutoff is 10 kHz. Since electron plasma frequencies this low are very rare in the solar wind, we currently do not have any suitable data for demonstrating the electrostatic character of the electron plasma oscillations. However, Rodriguez and Gurnett [1975], using data from the magnetic loop antenna on IMP 6, have shown that no appreciable signals are observed in the magnetic receiver at the electron plasma frequency when the electric receiver is observing electron plasma oscillations.

An expanded display of an electron enhancement event is shown in Figures 12. The enhanced electron fluxes appear in bursts. The upstream electron events have durations as short as a few seconds and typical durations of a few tens of seconds to a few minutes. The electron plasma oscillations are enhanced at the time the electron fluxes abruptly increase or decrease. Figures 10 and 12 clearly show that the more intense electron plasma oscillations tend to be associated with higher fluxes of low energy electrons. For example, from 1936 UT to 1953 UT, the flux of 1.4 to 1.6 keV electrons increases from about 2×10^3 to 1×10^4 $(cm^2\ sec\ ster\ keV)^{-1}$. During the same time interval the electron plasma oscillation amplitudes increase from about 60 $\mu V/m$ to

about 1 *mV/m*. Polarization measurements for electron plasma oscillations can be difficult to interpret due to the impulsive character of the waves. As shown in Figure 13a, the amplitude of electron plasma oscillations can change by more than two orders of magnitude in about a tenth of a second. In these examples the peak amplitude approaches 10 mV/m. The arrows along the top of Figures 13a and 13b show when the electric antenna is nearly parallel to the ambient magnetic field. For both examples the magnetic field was within a few degrees of the electric antenna spin plane. These four second rapid sample "snapshots" show that for the electron plasma oscillations the peak amplitudes usually occur near when the electric antenna is most nearly aligned with the static magnetic field.

The most likely mechanisms discussed for generating the electron plasma oscillations have been two-stream instabilities [Fredricks et al., 1971; Scarf et al., 1971] involving the solar wind and a suprathermal electron beam generated in or at the bow shock. The two-stream instability requires a positive slope in the velocity distribution function near the phase velocity of the waves. In order for the two-stream instability to produce electron plasma oscillations, a highly anisotropic suprathermal bump-on-tail electron distribution is required [Krall and Trivelpiece, 1973]. A secondary maximum in the distribution function caused by electrons from the bow shock has been observed by Gurnett and Frank [1975] simultaneously with intense electron plasma oscillations. The energy of the secondary maximum varies from several hundred eV to a few keV. Filbert and Kellogg [1979] suggest that the double-humped distribution function is probably produced by a time-of-flight mechanism in which, for energetic electrons generated at the

bow shock, the lower-energy electrons are swept downstream by the solar wind convection field and the remaining higher energy electrons leave a higher-energy bump on the distribution function.

We shall now compare our observations of electron plasma oscillations and the associated electron distribution function with the two-stream instability theory. The real part of the dispersion relation for longitudinal electron plasma oscillations can be written as

$$f^2 = f_p^2(1 + 3k^2/K_D^2)$$

where $K_D = 1/\lambda_D$, k is the wave number, $\lambda = 2\pi/k$ is the wave length, f_p is the electron plasma frequency, and the equation is valid over the range $0 < k < K_D$ [Scarf et al., 1971; Krall and Trivelpiece, 1973]. The phase velocity of the waves is $V_p = \omega/k = 2\pi f/k$. Examples of electron velocity distribution functions we measure when electron plasma oscillations are present are shown in Figure 14. Panel (a) contains data from 1031:39 UT to 1033:47 UT on November 6, 1977, and panel (b) contains data from 1035:36 to 1038:04 on the same day. At this time $\vec{B}$ is pointed toward the bow shock. Electron beams are evident in both panels along the negative $V_\parallel$ axis which is directed away from the bow shock. In panel (a) a positive slope in the parallel electron velocity distribution function is observed from -10.8×10^3 km/sec to -12.0×10^3 km/sec. These velocities are equivalent to electron energies of 330 eV and 410 eV, respectively. In panel (b) about four minutes later, a positive slope in the parallel electron velocity distribution function is observed from -19.8×10^3 km/sec to -21.0×10^3 km/sec. These velocities are equivalent to electron energies of 1.11 keV and 1.25 keV,

respectively. Not all electron velocity distribution functions measured while electron plasma oscillations occur show evidence of beams because the beams frequently fluctuate faster than the time required to produce a meaningful distribution function. The range of electron energies observed here is typical of the energies we find associated with the electron plasma oscillations.

We shall now calculate the wavelengths expected from these observations. Since the region of positive slope in the velocity distribution function equals the phase velocities of the waves, the wavelengths corresponding to 10.8×10^3 km/sec and 21.0×10^3 km/sec are 400 m and 780 m, respectively. These calculated wavelengths are much longer than our electric antennas which is in good agreement with our observations that the electron plasma oscillations have long wavelengths.

Substituting λ and λ_D into the dispersion relation we can calculate the frequency spread expected from the observed electron distribution function. Around 1035 UT November 6, 1977, the plasma frequency as determined from the sweep frequency receiver is 27 kHz which indicates a number density of 9 cm^{-3}. The electron temperature is 1.4×10^5 °K [J. D. Scudder, private communication]. These parameters yield a Debye length of 8.6 m. For $\lambda = 400$ m, $f \simeq 1.03\ f_p$. For $\lambda = 780$ m, $f \simeq 1.01\ f_p$. For a constant number density and electron beams with energies varying from a few hundred eV to slightly over 1 keV we thus expect a frequency spread in the electron plasma oscillations of only a few percent. This is in good agreement with our observations that the electron plasma oscillations have very narrow bandwidths. We attribute the large fluctuations in the center frequency of the narrowband emissions which are sometimes observed to fluctuations in the number density. The above

calculations have shown that our observations of nearly monochromatic long-wavelength electron plasma oscillations associated typically with electron beams of energy 0.2 to 1.5 keV are consistent with the two-stream instability theory. One aspect of our observations that yet needs explanation is the enhancement of the electron plasma oscillations at gradients in the energetic electron densities. The enhancements occur both at sharp increases and sharp decreases in the electron flux.

A thorough inspection of the spectrum analyzer data that contains electron plasma oscillations shows that additional waves almost always accompany the electron plasma oscillations. Whistler-mode waves and short-wavelength ion-acoustic waves that accompany electron plasma oscillations will be discussed in Section V. The waves we will discuss here are low-frequency electrostatic waves that have longer wavelengths and lower observed frequencies than the ion-acoustic waves we have already studied. Examples of these waves appear at and below 1.78 kHz around 1630 UT in Figure 10 and from 1936 to 1953 UT in Figure 12. The intensity of these waves correlates well with the intensity of the electron plasma oscillations. We have been very cautious in discussing these waves for fear that they may be a result of intense electron plasma oscillations saturating the preamplifiers and causing non-linear effects. We do not believe that these waves arise because of saturation effects for several reasons. The waves appear on both ISEE 1 and ISEE 2, even though the ISEE 2 antenna is seven times shorter and thus the signal at the preamplifier due to electron plasma oscillations is seven times smaller. The waves also appear even when the amplitude of the electron plasma oscillations is two or three orders of magnitude below where the preamplifiers could begin to saturate.

As shown in Figures 10 and 12, these low-frequency waves are very impulsive with peak amplitudes far exceeding the average amplitudes. No magnetic waves at the same frequencies are observed which indicates that the waves are electrostatic. These low-frequency electrostatic waves have frequencies which are usually lower than the Doppler-shifted ion-acoustic wave frequencies earlier studied. An example of the electric field spectra of the low frequency electrostatic waves is shown in Figure 11 below 3.1 kHz. The wave spectra do not display the broad peak found for the short-wavelength ion-acoustic waves, but rather monotonically increase with decreasing frequency. The peak spectral densities measured for the low frequency electrostatic waves on ISEE 1 and 2 are comparable across the frequency range where they are observed indicating that the wavelengths exceed 215 m. No short wavelength effects are observed. Because the waves are so impulsive, the average spectral densities shown in Figure 11 are controlled by the noise level of the two receivers and do not represent the spectra of the low-frequency electrostatic waves. These waves may be long-wavelength ion-acoustic waves.

The simultaneous observation of high frequency electron plasma oscillations and low-frequency electrostatic waves and ion-acoustic waves with the upstream electrons suggests that non-linear plasma processes are active. An instability that might be responsible for these low-frequency waves is the parametric decay instability examined extensively by Thornhill and ter Haar [1978], Nicholson and Goldman [1978] and Nicholson et al. [1978]. The parametric decay instability is active for longitudinal electron plasma oscillations (Langmuir waves) for wave numbers $k > 1/3\sqrt{\mu}/K_D$ where $\mu = m_e/m_i = 1/1837$ [Thornhill and ter Haar, 1978]. For this instability the Langmuir wave decays into

another Langmuir wave having almost the same frequency and an additional low-frequency wave. Both $\vec{k}$ and ω have to be conserved. For the solar wind conditions we have been investigating, a Langmuir wave being driven by a 1 keV electron beam would have $k \sim 3.5\sqrt{u}/K_D$ and a wavelength of 654 m. The wavelength of the first low-frequency decay product would not be short enough to account for the short-wavelength ion-acoustic waves but could account for the long wavelength low-frequency electrostatic waves we observed. However, since k is several times larger than $\sqrt{u}/K_D$, several decays could occur and the final low-frequency waves from the parametric decay instability could be the short-wavelength ion-acoustic waves.

V. WHISTLER-MODE WAVES

Electromagnetic waves with frequencies below 200 Hz are observed during almost all ion flux enhancement events. Figure 15 shows two one minute intervals of wideband analog data during an ion flux enhancement event illustrated in Figures 5 and 7. Several bursts of ion-acoustic waves are evident in the 0 to 10 kHz spectrograms. The electromagnetic waves are observed in the 0 to 500 Hz spectrograms as tones ranging in frequency from about 40 Hz to 80 Hz. At this time the electron gyrofrequency was about 140 Hz. Although the wideband analog receiver was connected to the electric antenna, the tones are electromagnetic as indicated by signals being present in the magnetic spectrum analyzer data at the appropriate frequency at the same time. As shown in the bottom panel of Figure 7, the magnetic spectrum analyzer signals are usually weak and very impulsive during the ion enhancement events. We measured the waves' indices of refraction by comparing their magnetic and electric signal strengths. This could not always be done because for the lowest frequencies the electric spectrum analyzer was dominated at low signal strengths by interference from the solar array. For the stronger signals when we could make the measurements, the results were compatible with whistler-mode waves. For example, the the strong tone at 2113:30 in Figure 15 was observable in the 56-Hz channel for both the electric and magnetic spectrum analyzers on ISEE 1 for two samples. The average magnetic field spectral density was $9.3 \times 10^{-5}\ \gamma^2/\text{Hz}$ and the average electric field spectral density was $3.5 \times 10^{-11}\ \text{V}^2/\text{m}^2\ \text{Hz}$. These values yield 489 as the measured index of refraction. The measured

index of refraction using the 56 Hz signal spectral densities for the tone at 2122:10 was 444. For whistler-mode propagation parallel to the ambient magnetic field the theoretical value of the index of refraction, n, is

$$n = \frac{f_p^2}{f(f_g - f)}^{1/2}$$

where f_g is the electron gyrofrequency. For f_p = 31 kHz, f_g = 140 Hz and f = 56 Hz, the conditions appropriate for these measurements, we find n = 452. Our identification of the signals as whistler-mode waves thus appears reasonable.

Typically, the whistler-mode waves observed during ion flux events occur between one-quarter and one-half the electron gyrofrequency. They last from 2 to 10 seconds and their center frequency drifts up or down in this time. These whistler-mode waves appear very similar to "lion roars" observed in the magnetosheath [Smith and Tsurutani, 1976] and, except for their low frequency, to whistler-mode chorus observed in the outer magnetosphere [Tsurutani and Smith, 1974] during substorm injection of plasma sheet electrons.

Figure 15 shows that the whistler-mode waves associated with enhanced ion flux events frequently occur during lulls in the ion-acoustic wave activity when the low energy ion fluxes are at a minimum. Occasionally, the low energy electron data show peaks coincident with the whistler-mode radiation. A survey of the high-time resolution particle data, when both electrons and ions were detected simultaneously during enhanced ion flux events, shows that the occurrence pattern is very complicated. On a macroscopic scale, intense whistler-mode waves

are typically associated with the more intense ion flux events as indicated in Figure 7. However on a microscopic scale, the electron spikes (and whistler-mode waves) observed tend to occur near minima of the ion fluxes. This relationship between electron spikes and ion flux levels was noted earlier by Lin et al. [1974] for the $\gtrsim$ 30 keV particles. These observations show that, although whistler-mode waves are observed associated with enhanced ion flux events, the smaller low energy electron flux enhancements accompanying the ion flux enhancements are possibly also related to the generation of the whistler-mode waves.

Although the examples we have shown in this section are for dispersed ion flux events, weak and impulsive whistler-mode turbulence also accompanies the presence of most ion beams. This is shown in Figure 8 where weak and sporadic whistler-mode waves from 5.6 Hz to 56 Hz occur for a 15-minute period coincident with an ion beam event. Whistler-mode waves becomes more intense and steady only in the presence of intense long-lasting beams. For the strong ion beam from 0340 to 0510 UT on October 27, 1978, shown in Plate 5 of Eastman et al. [1980], we observe steady and strong whistler-mode signals in our 100 Hz and 178 Hz channels. Peak spectral densities of 3.6×10^{-5} and 1.3×10^{-5} γ^2/Hz are observed for the two channels.

The whistler-mode waves could be caused by a cyclotron resonance involving the protons where the protons and the waves are moving in the same direction along the magnetic field. For waves much higher in frequency than the proton gyrofrequency, the parallel resonant energy for protons

$$E_R^+ \simeq \frac{m_p}{m_e} \frac{f}{f_g} \left(1 - \frac{f}{f_g}\right) E_B$$

[Smith and Tsurutani, 1976] where $E_B = B^2/8\pi N$, the magnetic energy per particle [Kennel and Petschek, 1966]. For $f = f_g/4$, $B = 5\gamma$ and $N = 10\ cm^{-3}$, $E_R^+ = 2.1$ keV. For $f = f_g/2$, $E_R^+ = 2.9$ keV. These energies are only slightly larger than the energies where we observe the largest ion flux enhancements.

The observed whistler-mode waves could also be generated by a streaming instability as suggested by Smith and Tsurutani [1976] for magnetosheath lion roars. A streaming instability can lead to wave growth when the velocity of the particles exceeds the phase velocity of the waves. The parallel phase velocity of whistler-mode waves is equal to the speed of light divided by the index of refraction. For an index of refraction of 500 which is typical for our observations, the phase velocity is 600 km/sec. For a proton this velocity represents an energy of 1.9 keV which is comparable to the energies of the ions having the largest fluxes during the ion flux enhancement events.

We also observe whistler-mode waves occasionally in the presence of electron plasma oscillations when energetic ions are absent. Electric and magnetic spectrum analyzer data for a two-minute period beginning at 1025 UT on November 6, 1977, are shown in Figure 16. From 1025:49 until 1026:47 we observe moderately intense-to-weak electron plasma oscillations in the 31 kHz electric field channel. At the same time in the 56 Hz and 100 Hz channels of both the electric and magnetic spectrum analyzers we observe whistler-mode waves. From 1 kHz to 5.6 kHz in the electric spectrum analyzer data we observe ion acoustic waves. The ion-acoustic waves peak in the 3.1-kHz channel on ISEE 1 and peak in the 5.6-kHz channel on ISEE 2. Figure 17 displays the 1.4 to 1.6 keV electron data and the wideband data during the time of the electron plasma

oscillations. The low energy electron flux abruptly increases coincident with the onset of the whistler-mode waves and the ion-acoustic waves. The low energy electron flux terminates coincident with the cessation of the whistler-mode waves and the ion-acoustic waves. Little activity was observed in the higher energy electron channels or in the ion data observed by the LEPEDEA and the Berkeley-Toulouse-Washington instruments at this time. If ions were responsible for the ion-acoustic wave activity at this time either they were below the energy range of the detectors or below the background intensity levels.

If the electron cyclotron resonance instability is responsible for the whistler-mode wave growth during ion enhancement events or electron plasma oscillation events, the ~ 1 keV electrons we observe are too high in energy to be the resonant electrons. The parallel resonant energy for electrons in cyclotron resonance with whistler-mode waves is $E_R^- = E_B \frac{f_g}{f}\left(1 - \frac{f}{f_g}\right)^3$ [Kennel and Petschek, 1966]. For B = 5γ and N = 10 cm^{-3}, the resonant energy for $f = f_g/2$ is 1.5 eV. Because this energy is far below the range of our instrumentation we cannot tell whether the low energy electron distribution is sufficiently anisotropic to support whistler-mode wave growth. The electrons we observe associated with whistler-mode waves might represent a high energy extension of the distribution that is directly responsible for the wave growth.

Correlated whistler-mode waves and electron plasma oscillation bursts have been detected on ISEE 3 far upstream of the Earth's bow shock by Kennel et al. [1980]. They suggested that whistler-mode waves and the electron plasma oscillations were not directly coupled but rather shared a common source of free energy, the electron heat flux. In one case they found good agreement between the observed whistler

frequency and the electron heat flux instability predictions of Gary and Feldman [1977]. They concluded that the electron plasma oscillations could be due to impulsive heating elsewhere on the field line connected to ISEE 3. The time of flight effect could then lead to a bump-on-tail distribution. In this research we are unable to clearly identify the source of the whistler-mode waves.

VI. SUMMARY AND DISCUSSION

In this study we have examined wave-particle interactions in the region upstream of the earth's bow shock using plasma wave and plasma data from the ISEE 1 and 2 spacecraft. The observation of simultaneous enhanced plasma wave activity and enhanced particle fluxes is a common feature of the upstream solar wind region especially on the dawn side. This is summarized in Figure 18 which contains data from the energetic particles and plasma wave electric field experiments for a 24 hour period outside the bow shock on November 9, 1977. All the particle data in this illustration came from detectors looking along the spin axis of the spacecraft. Lack of particle activity when plasma waves are active can be accounted for by the associated particle activity being at a lower energy or at a different pitch angle or of too low an intensity to be detected by the Berkeley-Toulouse-Washington instrument. For example, the three dimensional LEPEDEA instrument observed electron enhancement below 1 keV associated with the electron plasma oscillations observed in the 31 kHz plasma wave electric field data before 0100 UT and after 2300 UT when no electron flux enhancements are shown in the illustration. Enhanced particle fluxes in the upstream region occur when the solar wind magnetic field near the Earth is such that the spacecraft are in the ion foreshock region during ion flux enhancements or in the electron foreshock region during electron flux enhancements [Anderson et al., 1979; Eastman et al., 1980].

The predominant electrostatic waves associated with enhanced low energy ($\lesssim$ 1.5 keV) ion flux events are ion-acoustic waves. Wave spectra comparisons made between different length electric antennas on ISEE 1 and 2 show that the wavelengths are short and in the range from 30 to 215 meters. The resultant frequency spectra are then primarily due to Doppler shifts due to the solar wind flow. Wave polarization measurements for the ion-acoustic waves show that the electric field vectors are usually nearly parallel to the ambient magnetic field direction. Wave amplitudes increase with increasing ion flux and at spatial gradients in the energetic ion densities. The waves are very impulsive and the peak broadband amplitude is about 10 mV/m during very intense ion flux enhancement events. The same time offset between the two spacecraft for the ion flux structures and the ion-acoustic wave features indicates (1) that the waves are generated locally.

The predominant electrostatic plasma waves associated with enhanced electron flux events in the upstream solar wind are electron plasma oscillations. These long wavelength, nearly monochromatic waves are closely correlated with the flux of low energy (0.2 - 1.5 keV) electrons. The amplitudes of electron plasma oscillations are correlated with the fluxes of low energy electrons. Amplitudes near 10 mV/m have been observed. When only enhanced electron fluxes are present, the electron plasma oscillations are steady and the average amplitude approaches the peak amplitude. When the dispersed ion component is also present, however, the electron plasma oscillations decrease in amplitude and become more impulsive. The amplitudes of the electron plasma oscillations are enhanced at sharp gradients in the energetic electron densities. Wave polarization measurements for the electron plasma oscillations show that the peak amplitudes usually occur near where the

electric antenna is most nearly aligned with the static magnetic field. Whistler-mode waves, ion-acoustic waves, and/or low-frequency electrostatic waves usually accompany the electron plasma oscillations.

Weak and impulsive electromagnetic waves with frequencies below 200 Hz are observed during almost all ion flux enhancement events. The indices of refraction of these waves as determined by their wave B/E ratios are consistent with whistler-mode waves. They usually occur as one or more tones between $f_g/4$ and $f_g/2$. Proton cyclotron resonances and proton streaming instabilities were examined as possible generating mechanisms. High-time resolution comparisons of the wave and particle data indicate that the distribution of low energy electrons which accompanies the ion flux enhancement might also be related to the whistler-mode waves.

Three types of waves associated with electron plasma oscillations and/or the low energy electrons responsible for their growth are observed: whistler-mode waves, ion-acoustic waves and low-frequency electrostatic waves. We have shown that the parametric decay instability could produce ion-acoustic waves or the low frequency electrostatic waves.

In this report we have identified and examined in detail the plasma waves associated with the energetic plasma and particles upstream of the earth's bow shock and we have studied the wave particle interactions taking place between them. Many of the important observations we have used have been dependent on the multiple spacecraft concept of the ISEE mission. Multiple spacecraft, multiple antenna lengths, and high-time resolution measurements of the wave parameters and the 3-D particle velocity distributions are all essential for in depth studies of plasma waves and plasma in space.

ACKNOWLEDGEMENTS

We are grateful to K. A. Anderson for the high-time resolution particle data from the Berkeley-Washington-Toulouse experiments and to C. T. Russell for the UCLA magnetometer data which were used in this research . We wish to thank D. R. Nicholson, N. D'Angelo and H. Pesceli for many useful discussions. We are thankful for the computer data reduction assistance provided by B. G. Burek and T. Averkamp of the University of Iowa. This research was supported in part by the National Aeronautics and Space Administration under contract NAS5-20079 (University of Washington), contracts NAS5-20093, and NAS5-20094, and grants NGL-16-001-002 and NGL-16-001-043 (University of Iowa), and by the Office of Naval Research.

FIGURE CAPTIONS

Figure 1 Energetic ion fluxes and ISEE 2 plasma wave electric fields during an ion flux enhancement event. The electrostatic ion-acoustic waves occur simultaneously with the ion flux enhancement. Note how sporadic and impulsive the electron plasma oscillations are during the ion flux enhancement.

Figure 2 Energetic electron fluxes and ISEE 1 plasma wave electric fields for the same time period shown in Figure 1. The ion-acoustic wave amplitudes at higher frequencies on ISEE 1 are smaller because of their short wavelengths. The energetic electron fluxes are variable during the ion flux event but they fluctuate more sporadically and with less enhancement.

Figure 3 Electric field spectra for ISEE 1 and 2 during an ion flux enhancement event. The broad peak from 100 Hz to about 10 kHz is due to ion-acoustic waves. The difference in spectra above 300 Hz is due to the short wavelengths of the ion-acoustic waves.

Figure 4 Three one minute frequency-time spectrograms from ISEE 2 showing ion-acoustic waves observed during an ion flux enhancement event.

Figure 5 Energetic ion fluxes and ISEE 2 plasma wave electric fields during two ion flux enhancement events. Note that the ion-acoustic waves are greater during the more intense ion flux enhancement.

Figure 6 An expanded display of the energetic ion fluxes and plasma wave electric field data during the first ion flux enhancement event in Figure 5. The wave amplitudes tend to peak near particle flux gradients.

Figure 7 Energetic electron fluxes and ISEE 1 plasma wave electric and magnetic fields for the same time period as Figure 5. The shaded areas indicate the times of the ion flux enhancement events. Weaker and more sporadic electron flux enhancements and whistler-mode turbulence both occur coincident with the ion flux enhancements.

Figure 8 ISEE 1 plasma wave electric and magnetic field data for one hour on November 6, 1977. Ion-acoustic waves and impulsive whistler-mode radiation are observed from 2335 UT to 2350 UT coincident with an ion beam event shown in [Eastman et al., 1980, Plate 1].

Figure 9 Two examples of rapid sample electric field data for ion-acoustic waves. The arrows indicate when the spinning electric antenna was most nearly aligned with the ambient magnetic field. Panel (a) contains 3.1 kHz data sampled 32 times per second. The ambient magnetic field was pointed antisunward and about 15° below the ecliptic plane. Panel (b) contains 5.6 kHz data sampled 8 times per second. The solar wind magnetic field was within a few degrees of the ecliptic plane. The peak amplitudes for the ion-acoustic waves usually occur when the antenna is most nearly aligned to the ambient magnetic field.

Figure 10 Energetic electron fluxes and ISEE 2 plasma wave electric field data showing the association of electron fluxes and electron plasma oscillations.

Figure 11 Electric field spectra for ISEE 1 and 2 during an electron flux enhancement event which show that the electron plasma oscillations have the same field strengths as measured by the 30 m and 215 m antennas.

Figure 12 An expanded display of energetic electron fluxes and ISEE 1 plasma wave electric field data during an electron flux event. Note how the more intense electron plasma oscillations tend to be associated with higher fluxes of low energy electrons. The electron plasma oscillations and low frequency electrostatic waves are also enhanced at gradients in the energetic electron density.

Figure 13 Two examples of the 31 kHz electric field rapid sample data for electron plasma oscillations. The arrows indicate when the spinning electric antenna was most nearly aligned with the ambient magnetic field. For both panels the magnetic field was oriented within a few degrees of the electric antenna spin plane. The peak amplitudes of the electron plasma oscillations usually occur near where the electric antenna is most nearly aligned with the static magnetic field. These panels also illustrate that the electron plasma oscillation amplitudes can rise or fall more than an order of magnitude in a tenth of a second.

Figure 14 Perspective plots of electron velocity distribution functions observed associated with upstream electron plasma oscillations on November 6, 1977, from 1031:39 UT to 1033:47 UT in panel (a) and from 1035:36 UT to 1038:04 UT in panel (b). Electron beams are evident in both panels along the negative $V_{\parallel}$ axis which is directed away from the bow shock. The parallel velocities of the beams are 1.2×10^4 km/sec and 2.1×10^4 km/sec, respectively.

Figure 15 Two one minute sets of plasma wave frequency-time spectrograms showing whistler-mode waves and ion-acoustic waves that occur during an ion flux enhancement event. The whistler-mode waves usually occur during lulls in the ion-acoustic wave activity.

Figure 16 ISEE 1 plasma wave electric and magnetic field data for two minutes on November 6, 1977, showing the association of electron plasma oscillations, ion-acoustic waves and whistler-mode radiation during a weak electron flux enhancement event.

Figure 17 Low energy electron flux and plasma wave wideband analog data during the weak electron flux enhancement event in Figure 16. Both multi-frequency whistler-mode radiation and ion-acoustic waves accompany the slightly enhanced low energy electron flux event. No enhancement in ion flux is evident.

Figure 18 A 24 hour summary plot of the energetic electron and ion fluxes and the plasma wave data for November 9, 1977. ISEE 1 and 2 were near apogee upstream of the bow shock during local morning. The low energy electron fluxes are well correlated with the electron plasma oscillations and low-frequency electrostatic waves. The low energy ions are well correlated with ion-acoustic waves.

REFERENCES

Anderson, K. A., R. P. Lin, R. J. Paoli, G. K. Parks, C. S. Lin, H. Reme, J. M. Bosgued, F. Martel, F. Cotin, and A. Cros, An experiment to study energetic particle fluxes in and beyond the Earth's outer magnetosphere, IEEE Trans. Geosci. Electr., GE-16, 213, 1978.

Anderson, K. A., R. P. Lin, F. Martel, C. S. Lin, G. K. Parks, and H. Reme, Thin sheets of energetic electrons upstream from the Earth's bow shock, Geophys. Res. Lett., 6, 401, 1979.

Eastman, T. E., R. R. Anderson, L. A. Frank, and G. K. Parks, Upstream particles observed in the Earth's foreshock region, submitted to J. Geophys. Res., 1980.

Filbert, Paul C., and Paul J. Kellogg, Electrostatic noise at the plasma frequency beyond the Earth's bow shock, J. Geophys. Res., 84, 1369, 1979.

Frank, L. A., D. M. Yeager, H. D. Owens, K. L. Ackerson, and M. R. English, Quadrispherical LEPEDEAS for ISEE's-1 and -2 plasma measurements, IEEE Trans. Geosci. Electr., GE-16, 221, 1978a.

Frank, L. A., K. L. Ackerson, R. J. DeCoster, and B. G. Burek, Three-dimensional plasma measurements within the Earth's magnetosphere, Space Sci. Rev., 22, 739, 1978b.

Fredricks, R. W., C. F. Kennel, F. L. Scarf, G. M. Crook, and I. M. Green, Detection of electric-field turbulence in the Earth's bow shock, Phys. Rev. Lett., 21, 1761, 1968.

Fredricks, R. W., F. L. Scarf, and L. A. Frank, Nonthermal electrons and high-frequency waves in the upstream solar wind, 2. Analysis and interpretation, J. Geophys. Res., 76, 6691, 1971.

Gary, S. Peter, and W. C. Feldman, Solar wind heat flux regulation by the whistler instability, J. Geophys. Res., 82, 1087, 1977.

Gary, S. Peter, Microinstabilities upstream of the earth's bow shock: A brief review, submitted to J. Geophys. Res., 1980.

Gurnett, D. A., and L. A. Frank, Electron plasma oscillations associated with type III radio emissions and solar electrons, Solar Phys., 45, 477, 1975.

Gurnett, D. A., and L. A. Frank, Ion acoustic waves in the solar wind, J. Geophys. Res., 83, 58, 1978.

Gurnett, D. A., F. L. Scarf, R. W. Fredricks, and E. J. Smith, The ISEE-1 and ISEE-2 plasma wave investigation, IEEE Trans. Geosci. Electr., GE-16, 225, 1978.

Gurnett, D. A., R. R. Anderson, F. L. Scarf, R. W. Fredricks, and E. J. Smith, Initial results from the ISEE-1 and -2 plasma wave investigation, Space Sci. Rev., 23, 103, 1979.

Kennel, C. F., and H. E. Petschek, Limit on stably trapped particle fluxes, J. Geophys. Res., 71, 1, 1966.

Kennel, C. F., F. L. Scarf, F. V. Coroniti, R. W. Fredricks, D. A. Gurnett, and E. J. Smith, Correlated whistler and electron plasma oscillation bursts detected on ISEE-3, Geophys. Res. Lett., 7, 129, 1980.

Krall, N. A., and A. W. Trivelpiece, Principles of Plasma Physics, p. 458, McGraw-Hill, New York, 1973.

Lin, R. P., C. I. Meng, and K. A. Anderson, 30- to 100-keV protons upstream from the Earth's bow shock, J. Geophys. Res., 79, 489, 1974.

Nicholson, D. R., and M. V. Goldman, Cascade and collapse of Langmuir waves in two dimensions, Phys. Fluids, 21, 1766, 1978.

Nicholson, D. R., M. V. Goldman, P. Hoyng, and J. C. Weatherall, Nonlinear Langmuir waves during type III solar radio bursts, Ap. J., 223, 605, 1978.

Parks, G. K., C. Gurgiolo, C. S. Lin, K. A. Anderson, R. P. Lin, F. Martel and H. Reme, Dual spacecraft observations of energetic particles in the vicinity of the magnetopause, bow shock, and the interplanetary medium, Space Sci. Rev., 22, 765, 1978.

Parks, G. K., E. Greenstadt, C. S. Wu, C. S. Lin, A. St-Marc, R. P. Lin, K. A. Anderson, C. Gurgiolo, B. Mauk, H. Reme, R. R. Anderson, and T. Eastman, Upstream particle spatial gradients and plasma waves, submitted to J. Geophys. Res., 1980.

Paschmann, G., N. Sckopke, S. J. Bame, J. R. Asbridge, J. T. Gosling, C. T. Russell, and E. W. Greenstadt, Association of low-frequency waves with suprathermal ions in the upstream solar wind, Geophys. Res. Lett., 6, 209, 1979.

Rodriguez, Paul, and Donald A. Gurnett, Electrostatic and electromagnetic turbulence associated with the Earth's bow shock, J. Geophys. Res., 80, 19, 1975.

Scarf, F. L., R. W. Fredricks, L. A. Frank, C. T. Russell, P. J. Coleman, Jr., and M. Neugebauer, Direct correlations of large-amplitude waves with suprathermal protons in the upstream solar wind, J. Geophys. Res., 75, 7316, 1970.

Scarf, F. L., R. W. Fredricks, L. A. Frank, and M. Neugebauer, Nonthermal electrons and high frequency waves in the upstream solar wind, 1. Observations, J. Geophys. Res., 76, 5162, 1971.

Smith, E. J., and Bruce T. Tsurutani, Magnetosheath lion roars, J. Geophys. Res., 81, 2261, 1976.

Stix, T. H., The theory of plasma waves, p. 132, McGraw-Hill, New York, 1962.

Thornhill, S. G., and D. ter Haar, Langmuir turbulence and modulational instability, Phys. Reports, 43, 43, 1978.

Tsurutani, Bruce T., and Edward J. Smith, Postmidnight chorus: A substorm phenomenon, J. Geophys. Res., 79, 118, 1974.

Wu, C. S., C. S. Lin, and H. Wong, Plasma waves excited by density gradients of upstream particles, to be submitted to J. Geophys. Res., 1980.

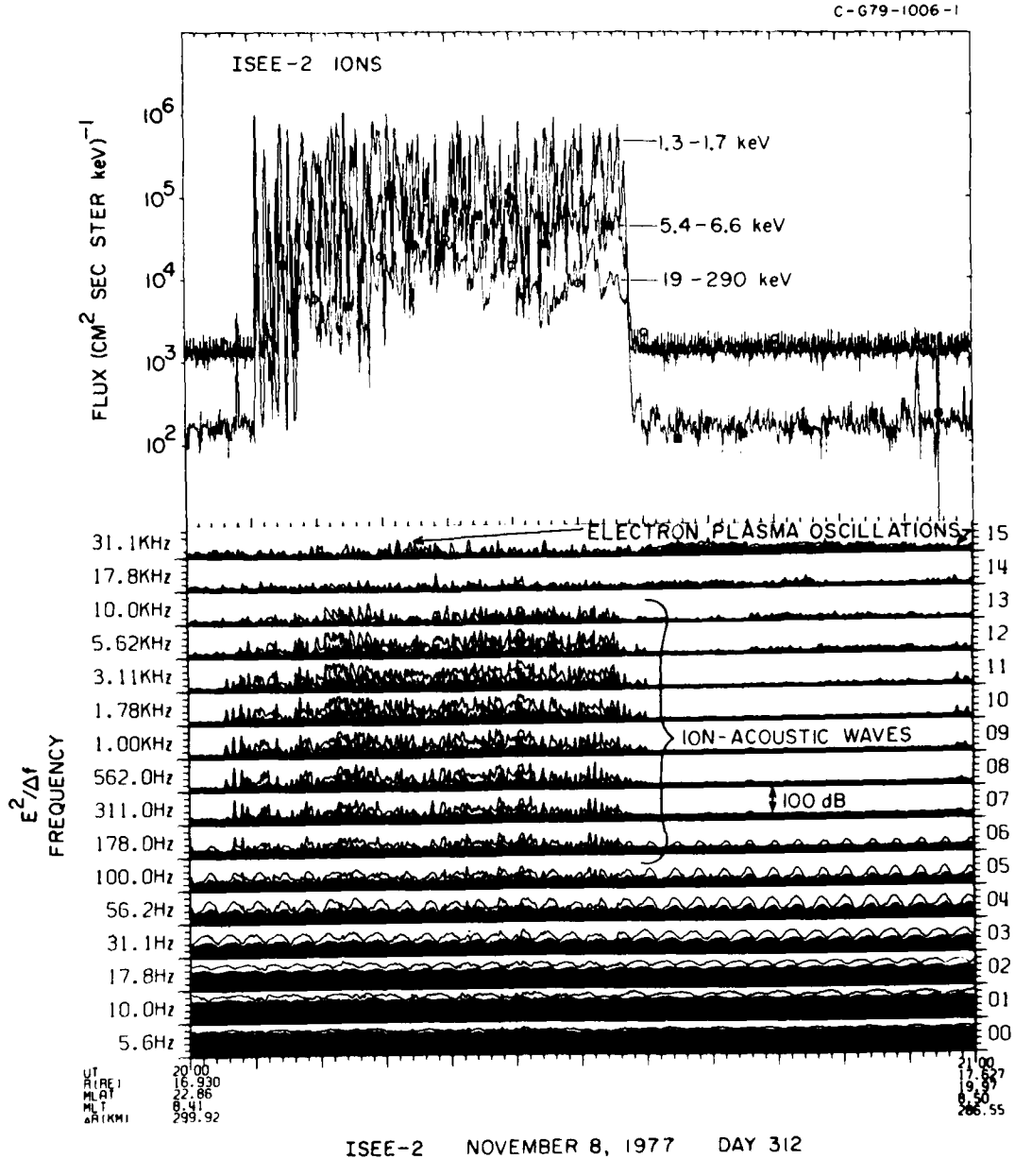
C-G79-1006-1
ISEE-2 IONS
FLUX (CM^2 SEC STER keV)$^{-1}$
10^6
10^5
10^4
10^3
10^2
1.3-1.7 keV
5.4-6.6 keV
19-290 keV
ELECTRON PLASMA OSCILLATIONS
ION-ACOUSTIC WAVES
100 dB
$E^2/\Delta f$
FREQUENCY
31.1KHz
17.8KHz
10.0KHz
5.62KHz
3.11KHz
1.78KHz
1.00KHz
562.0Hz
311.0Hz
178.0Hz
100.0Hz
56.2Hz
31.1Hz
17.8Hz
10.0Hz
5.6Hz
15
14
13
12
11
10
09
08
07
06
05
04
03
02
01
00
UT
R(RE)
MLAT
MLT
R(KM)
20:00
16.930
22.86
8.41
299.92
21:00
17.827
19.97
8.50
286.55
ISEE-2 NOVEMBER 8, 1977 DAY 312

Figure 1

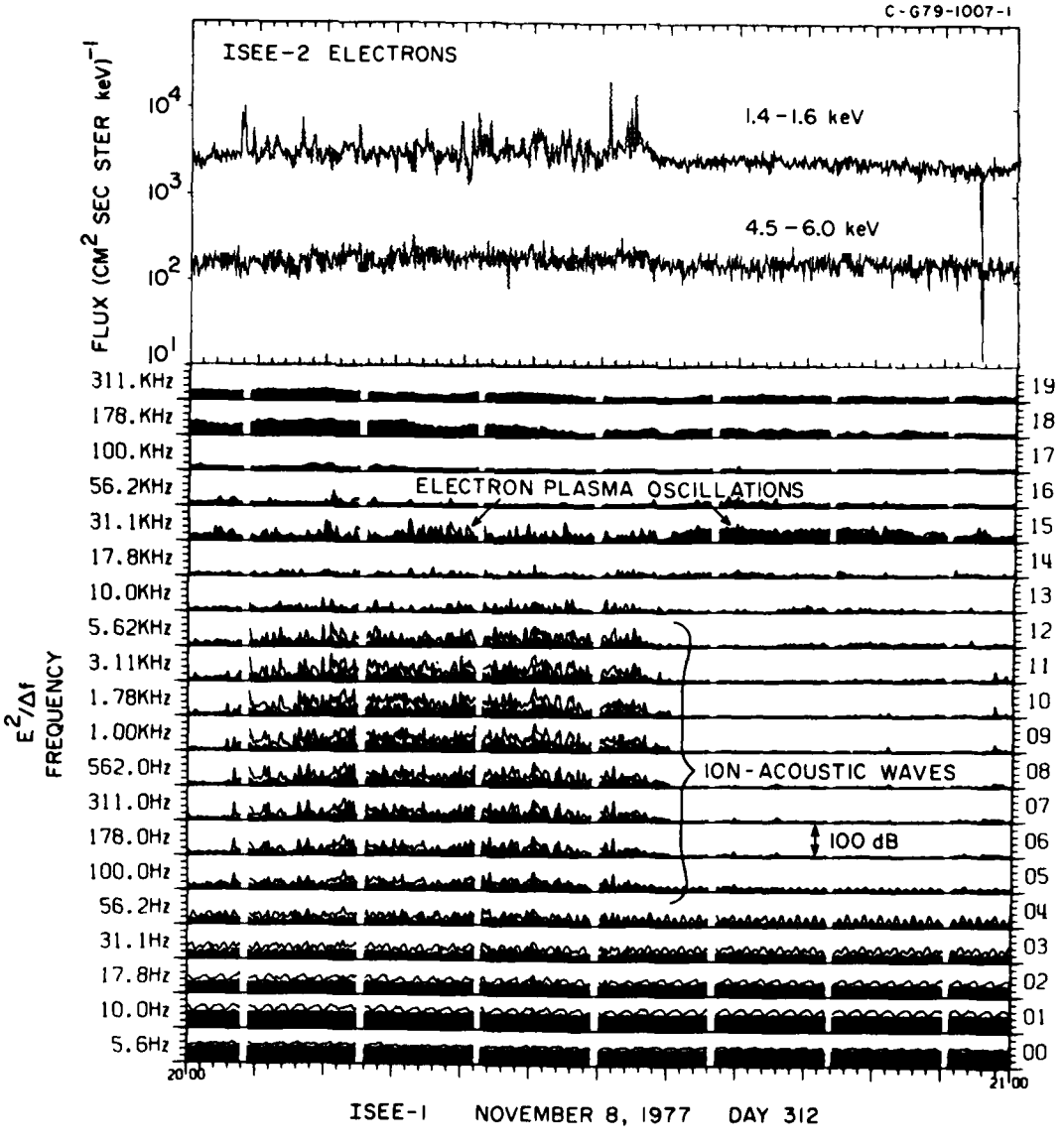
C-G79-1007-1
ISEE-2 ELECTRONS
1.4 - 1.6 keV
4.5 - 6.0 keV
FLUX (CM² SEC STER keV)⁻¹
10⁴
10³
10²
10¹
311.KHz
178.KHz
100.KHz
56.2KHz
31.1KHz
17.8KHz
10.0KHz
5.62KHz
3.11KHz
1.78KHz
1.00KHz
562.0Hz
311.0Hz
178.0Hz
100.0Hz
56.2Hz
31.1Hz
17.8Hz
10.0Hz
5.6Hz
E²/Δf
FREQUENCY
ELECTRON PLASMA OSCILLATIONS
ION-ACOUSTIC WAVES
100 dB
19
18
17
16
15
14
13
12
11
10
09
08
07
06
05
04
03
02
01
00
20⁰⁰
21⁰⁰
ISEE-1 NOVEMBER 8, 1977 DAY 312

Figure 2

A-G80-414-1

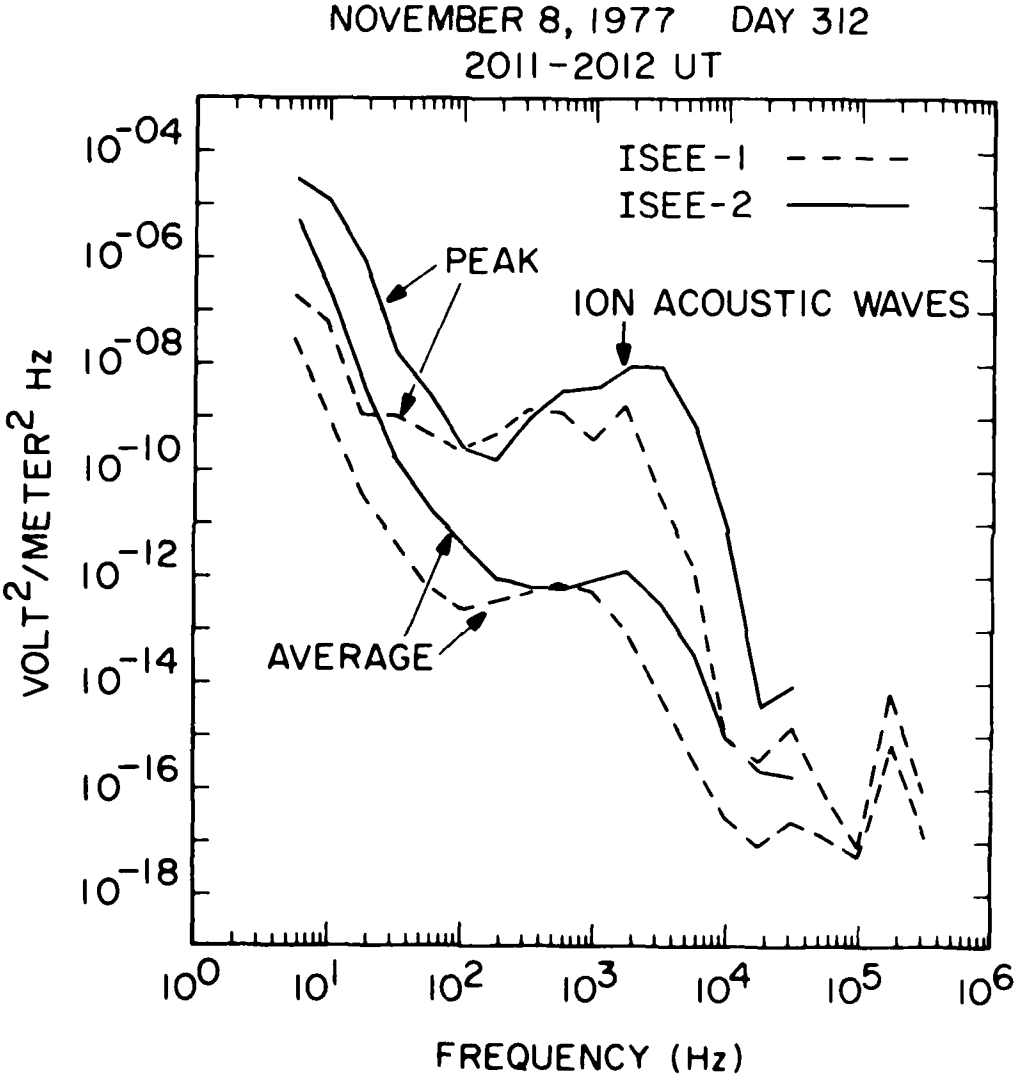

Figure 3

C-G80-634

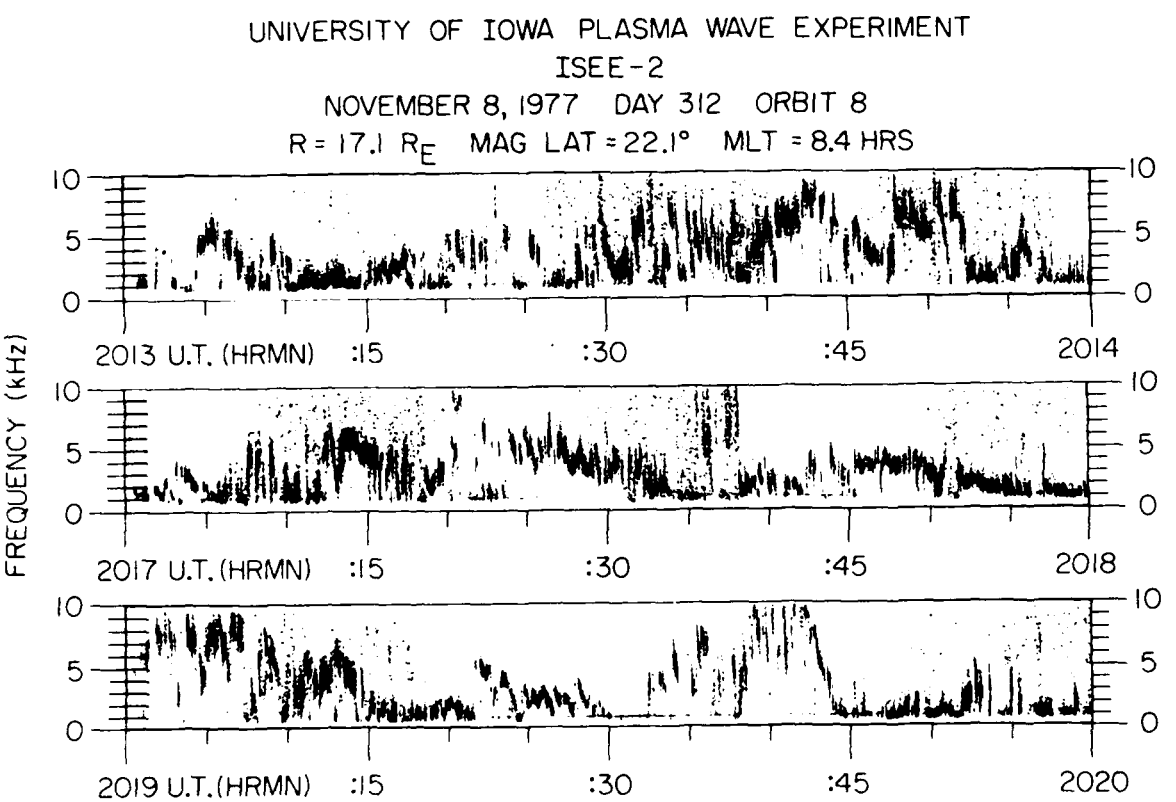

Figure 4

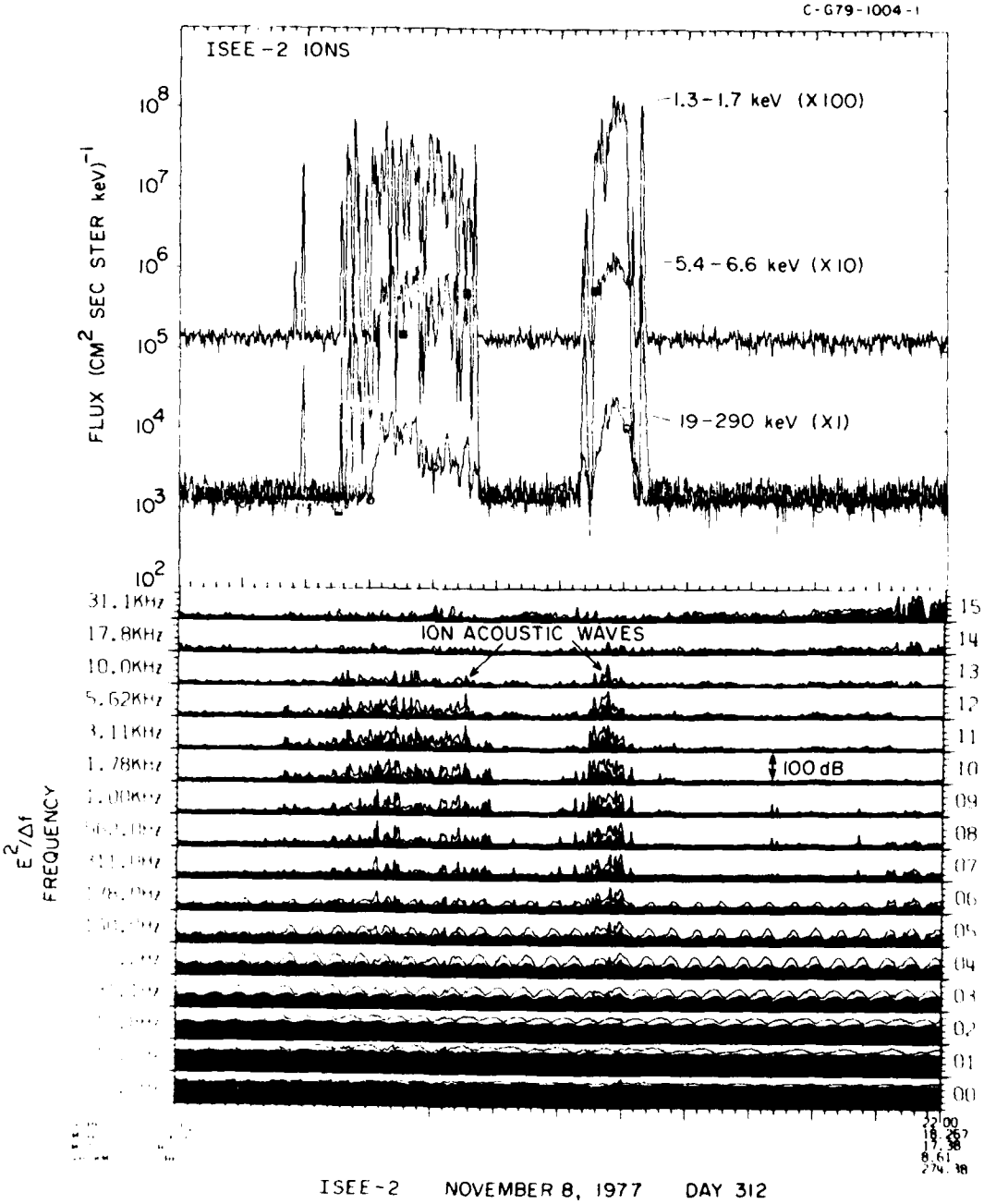
C-G79-1004-1
ISEE-2 IONS
1.3-1.7 keV (X100)
5.4-6.6 keV (X10)
19-290 keV (X1)
FLUX (CM^2 SEC STER keV)$^{-1}$
10^8
10^7
10^6
10^5
10^4
10^3
10^2
31.1KHz
17.8KHz
10.0KHz
5.62KHz
3.11KHz
1.78KHz
ION ACOUSTIC WAVES
100 dB
$E^2/\Delta f$
FREQUENCY
15
14
13
12
11
10
09
08
07
06
05
04
03
02
01
00
ISEE-2 NOVEMBER 8, 1977 DAY 312

Figure 5

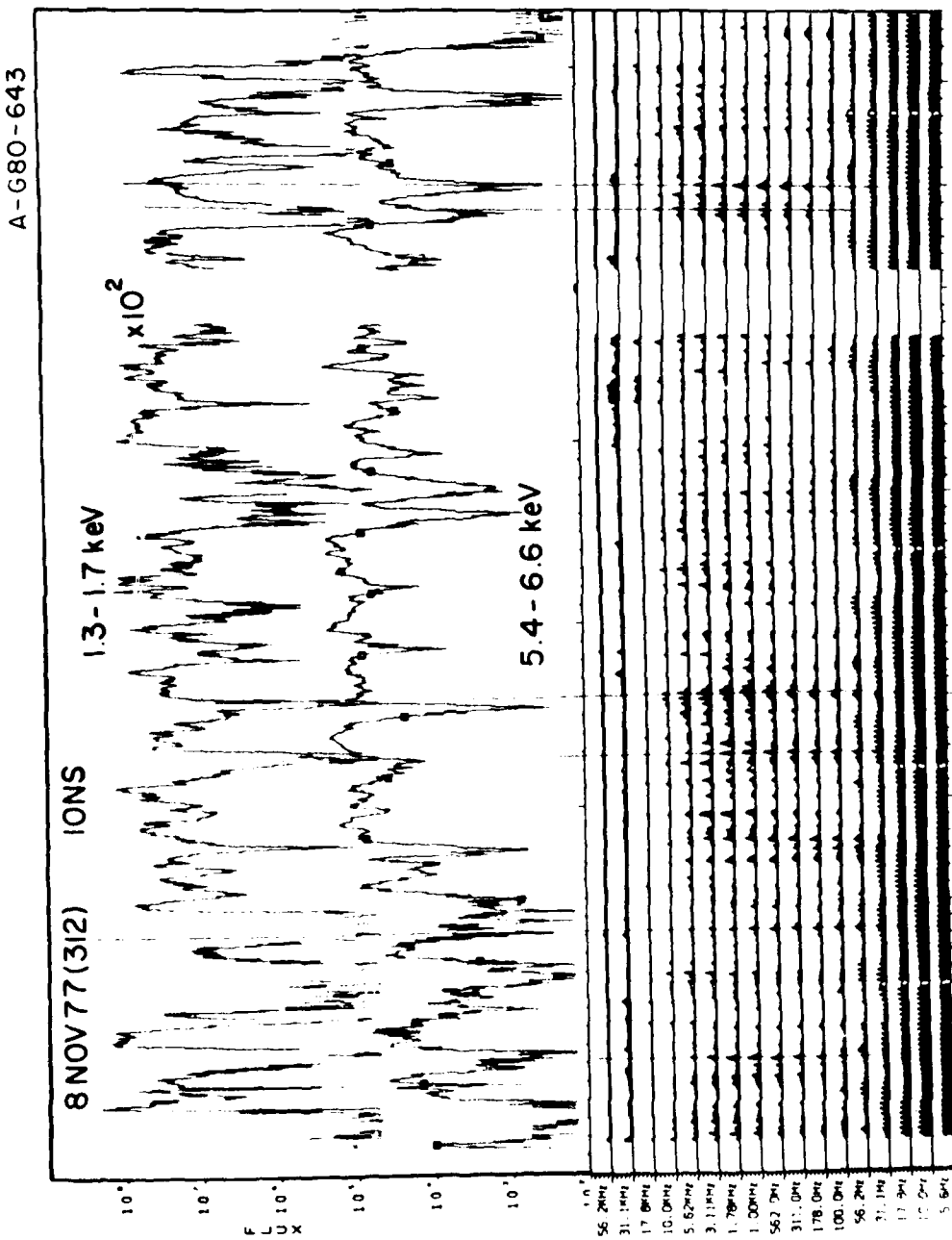
A-G80-643
8 NOV 77 (312) IONS
1.3-1.7 keV
x10²
5.4-6.6 keV
FLUX
2115
2120
UNIVERSAL TIME

Figure 6

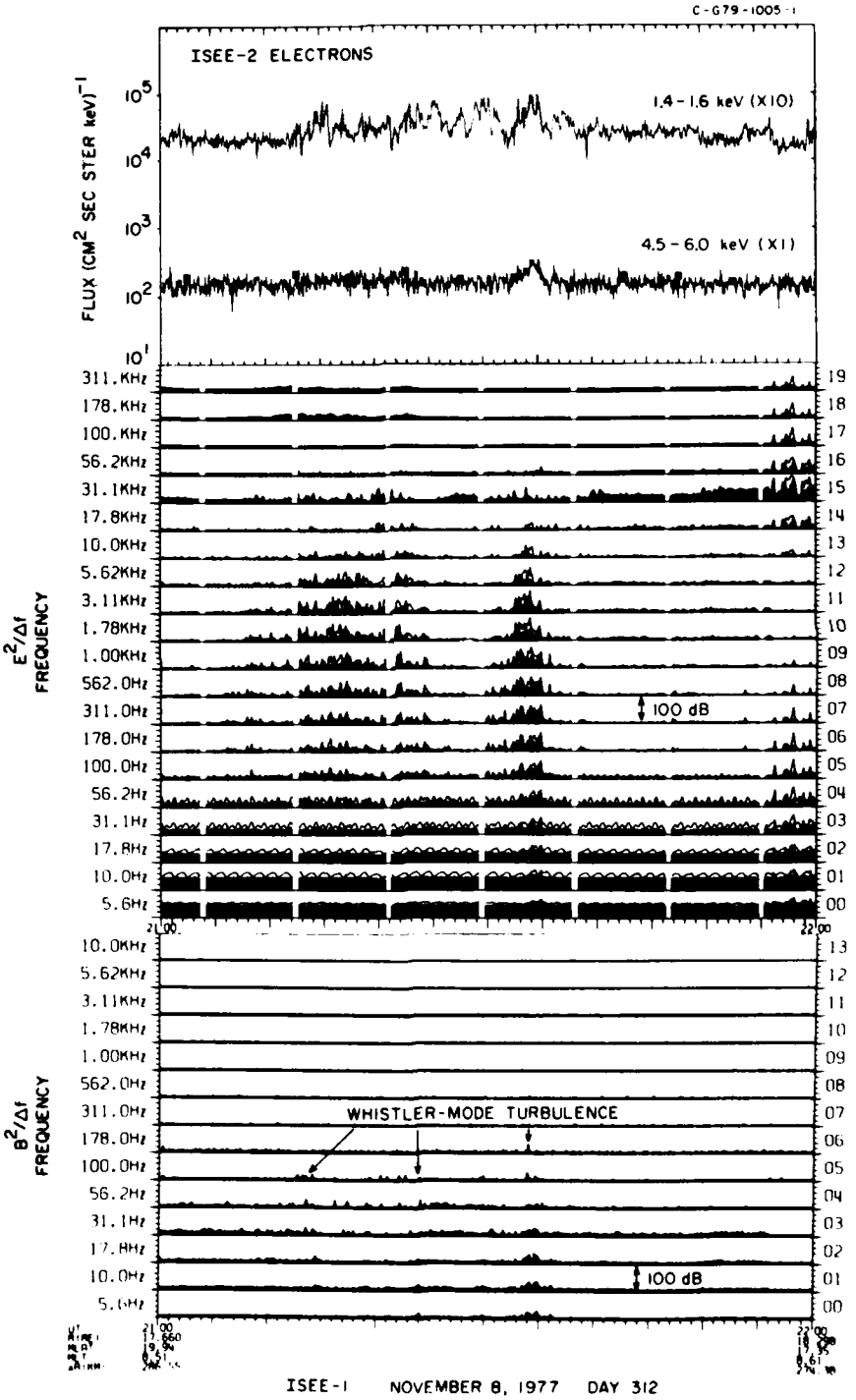
C-G79-1005-1
ISEE-2 ELECTRONS
1.4 - 1.6 keV (X10)
4.5 - 6.0 keV (X1)
FLUX (CM² SEC STER keV)⁻¹
E²/Δf FREQUENCY
B²/Δf FREQUENCY
100 dB
WHISTLER-MODE TURBULENCE
ISEE-1 NOVEMBER 8, 1977 DAY 312

Figure 7

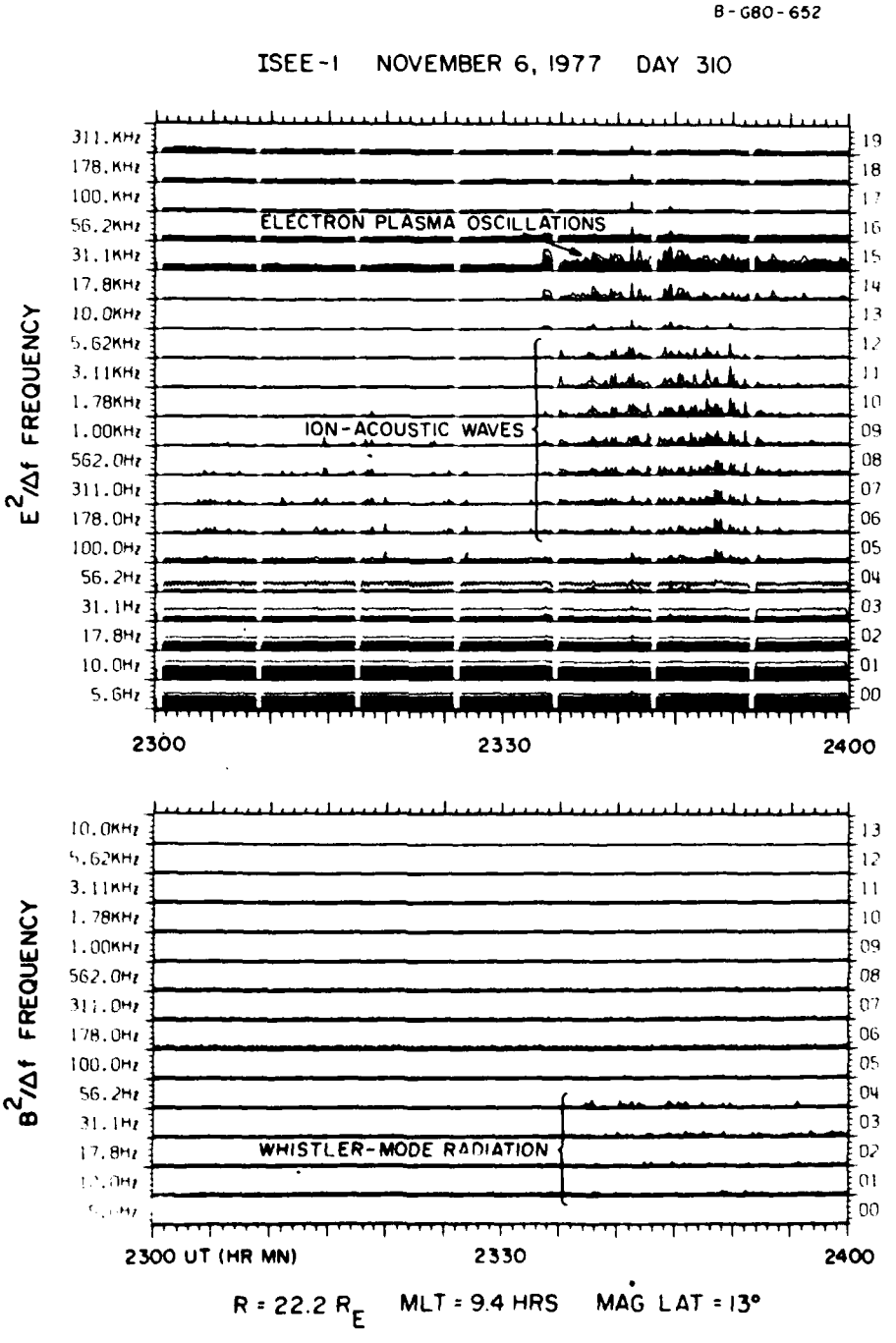
B-G80-652
ISEE-1 NOVEMBER 6, 1977 DAY 310
E²/Δf FREQUENCY
311.KHz
178.KHz
100.KHz
56.2KHz
31.1KHz
17.8KHz
10.0KHz
5.62KHz
3.11KHz
1.78KHz
1.00KHz
562.0Hz
311.0Hz
178.0Hz
100.0Hz
56.2Hz
31.1Hz
17.8Hz
10.0Hz
5.6Hz
19
18
17
16
15
14
13
12
11
10
09
08
07
06
05
04
03
02
01
00
ELECTRON PLASMA OSCILLATIONS
ION-ACOUSTIC WAVES
2300
2330
2400
B²/Δf FREQUENCY
10.0KHz
5.62KHz
3.11KHz
1.78KHz
1.00KHz
562.0Hz
311.0Hz
178.0Hz
100.0Hz
56.2Hz
31.1Hz
17.8Hz
13
12
11
10
09
08
07
06
05
04
03
02
01
00
WHISTLER-MODE RADIATION
2300 UT (HR MN)
2330
2400
R = 22.2 R_E MLT = 9.4 HRS MAG LAT = 13°

Figure 8

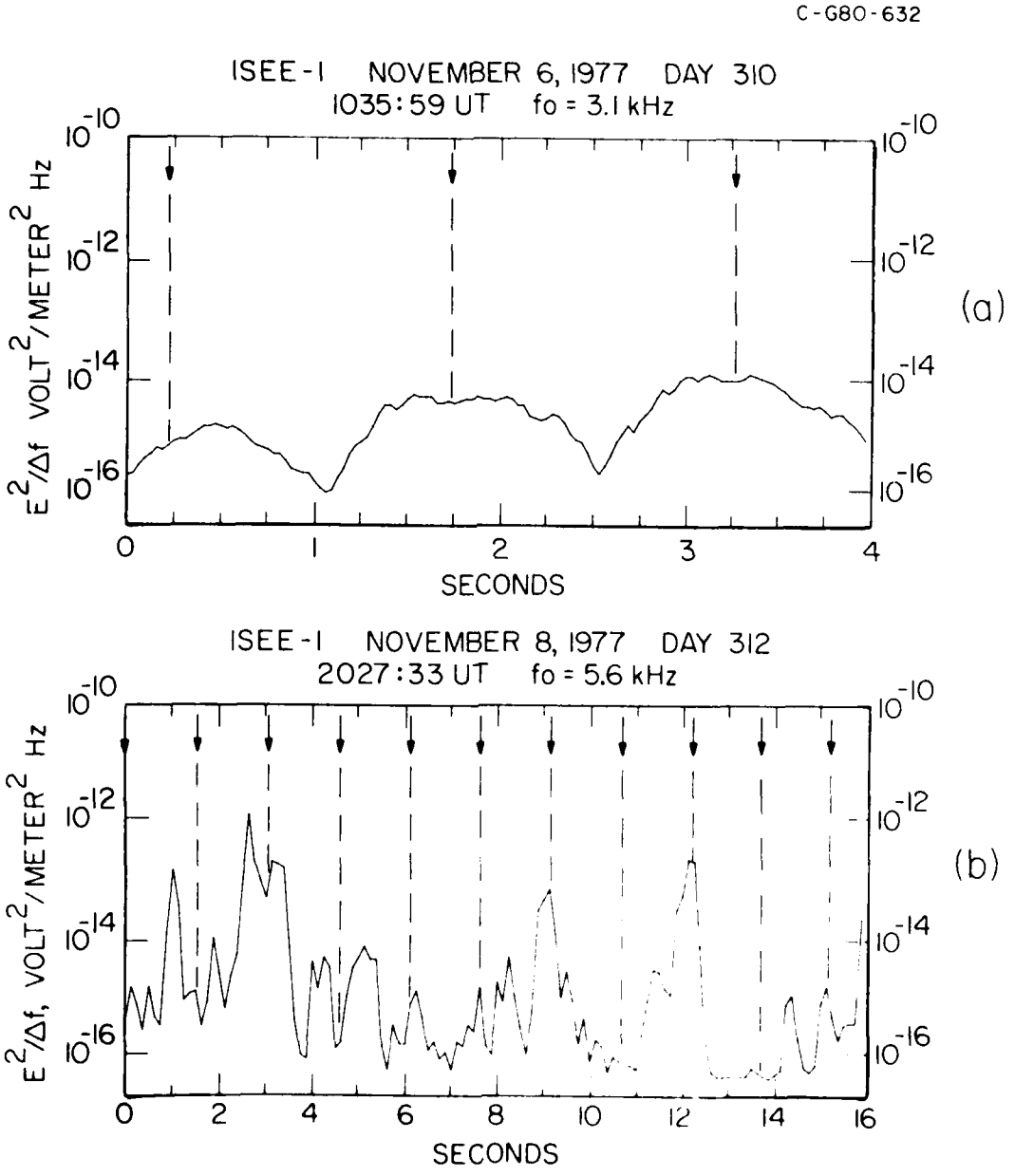
C-G80-632
ISEE-1 NOVEMBER 6, 1977 DAY 310
1035:59 UT fo = 3.1 kHz
$E^2/\Delta f$ VOLT^2/METER^2 Hz
10^{-10}
10^{-12}
10^{-14}
10^{-16}
0 1 2 3 4
SECONDS
(a)
ISEE-1 NOVEMBER 8, 1977 DAY 312
2027:33 UT fo = 5.6 kHz
$E^2/\Delta f$, VOLT^2/METER^2 Hz
10^{-10}
10^{-12}
10^{-14}
10^{-16}
0 2 4 6 8 10 12 14 16
SECONDS
(b)

Figure 9

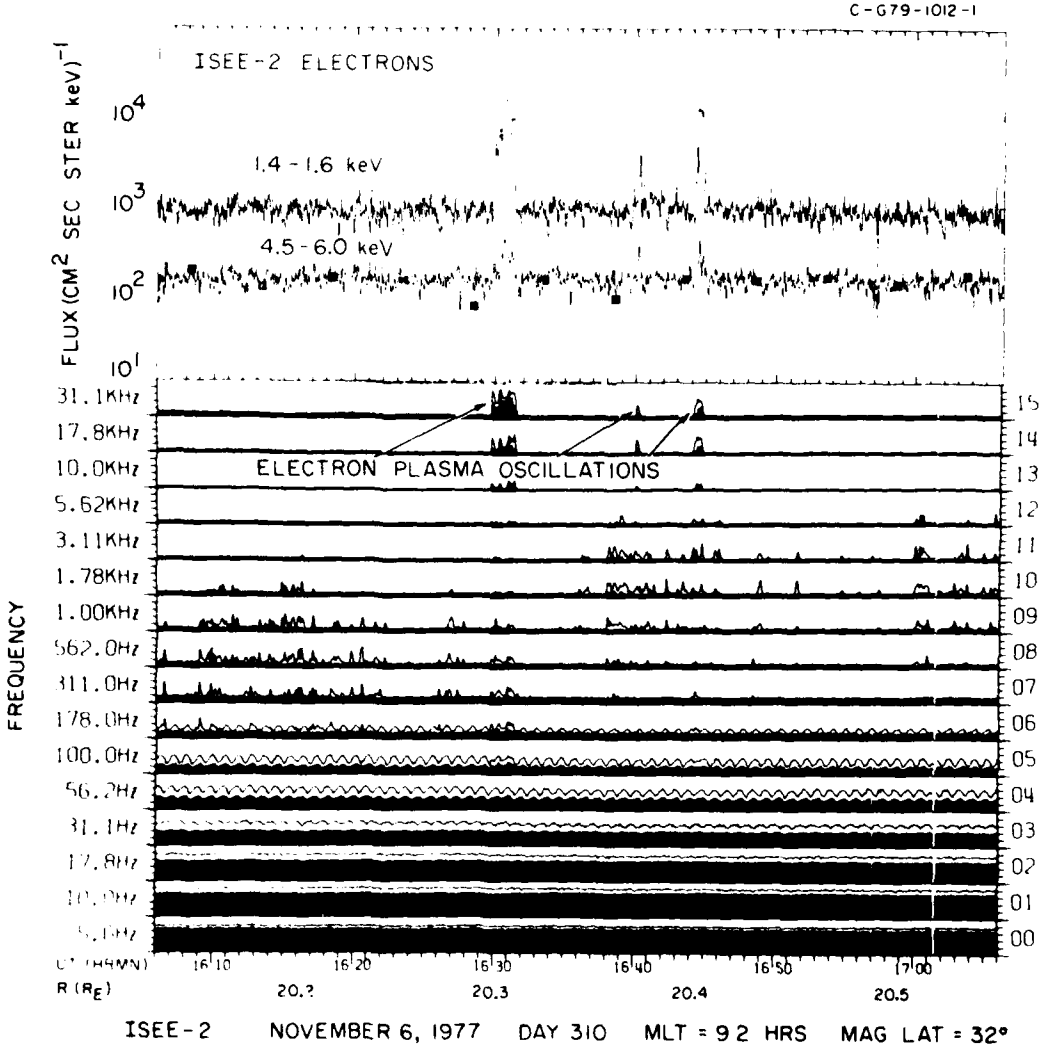
C-G79-1012-1
ISEE-2 ELECTRONS
FLUX (CM² SEC STER keV)⁻¹
10⁴
10³
10²
10¹
1.4 - 1.6 keV
4.5 - 6.0 keV
31.1KHz
17.8KHz
10.0KHz
5.62KHz
3.11KHz
1.78KHz
1.00KHz
562.0Hz
311.0Hz
178.0Hz
100.0Hz
56.2Hz
31.1Hz
17.8Hz
10.0Hz
5.6Hz
FREQUENCY
ELECTRON PLASMA OSCILLATIONS
15
14
13
12
11
10
09
08
07
06
05
04
03
02
01
00
16'10
16'20
16'30
16'40
16'50
17'00
R (RE)
20.2
20.3
20.4
20.5
ISEE-2 NOVEMBER 6, 1977 DAY 310 MLT = 9.2 HRS MAG LAT = 32°

Figure 10

A-G80-413-2

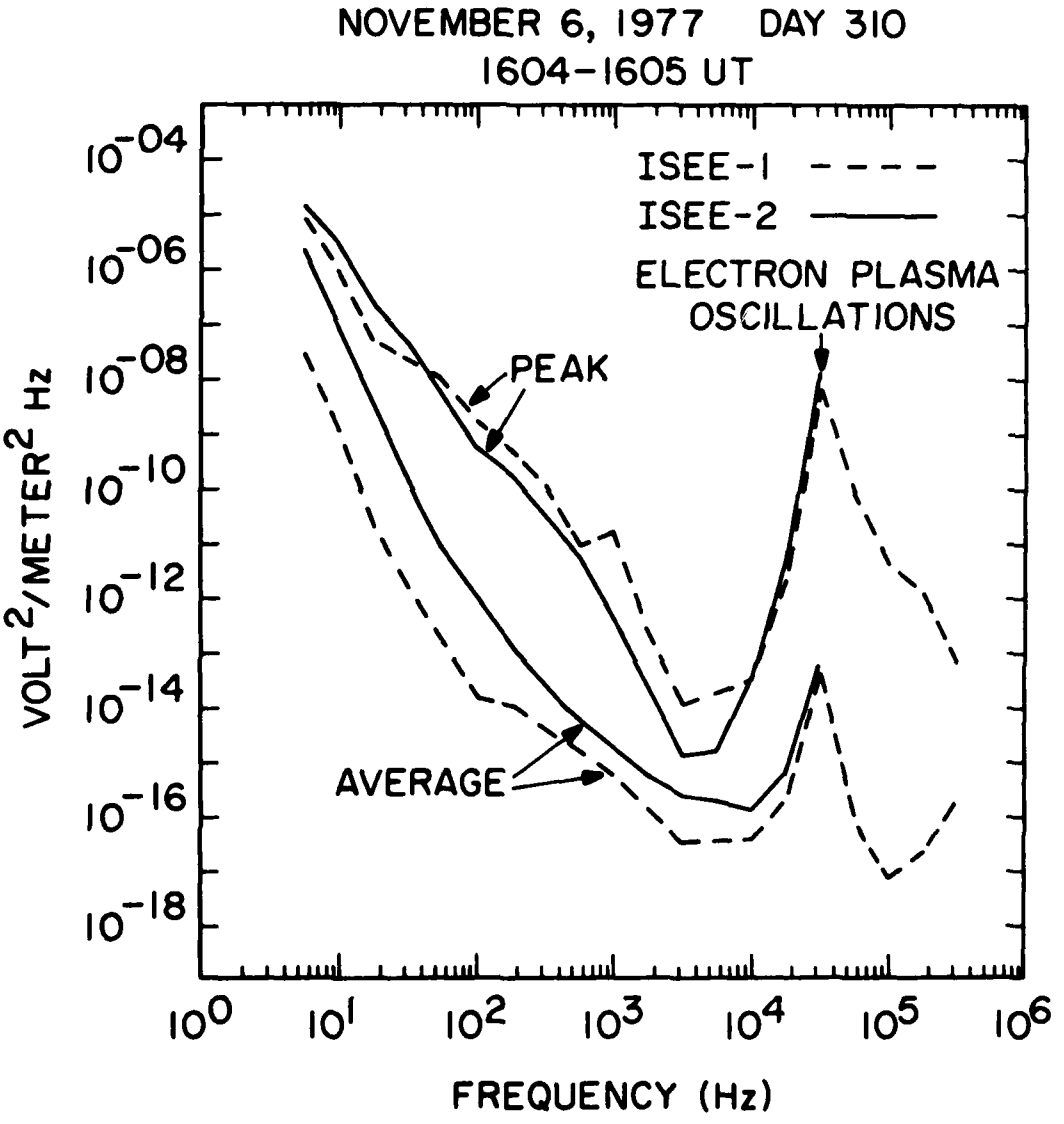

Figure 11

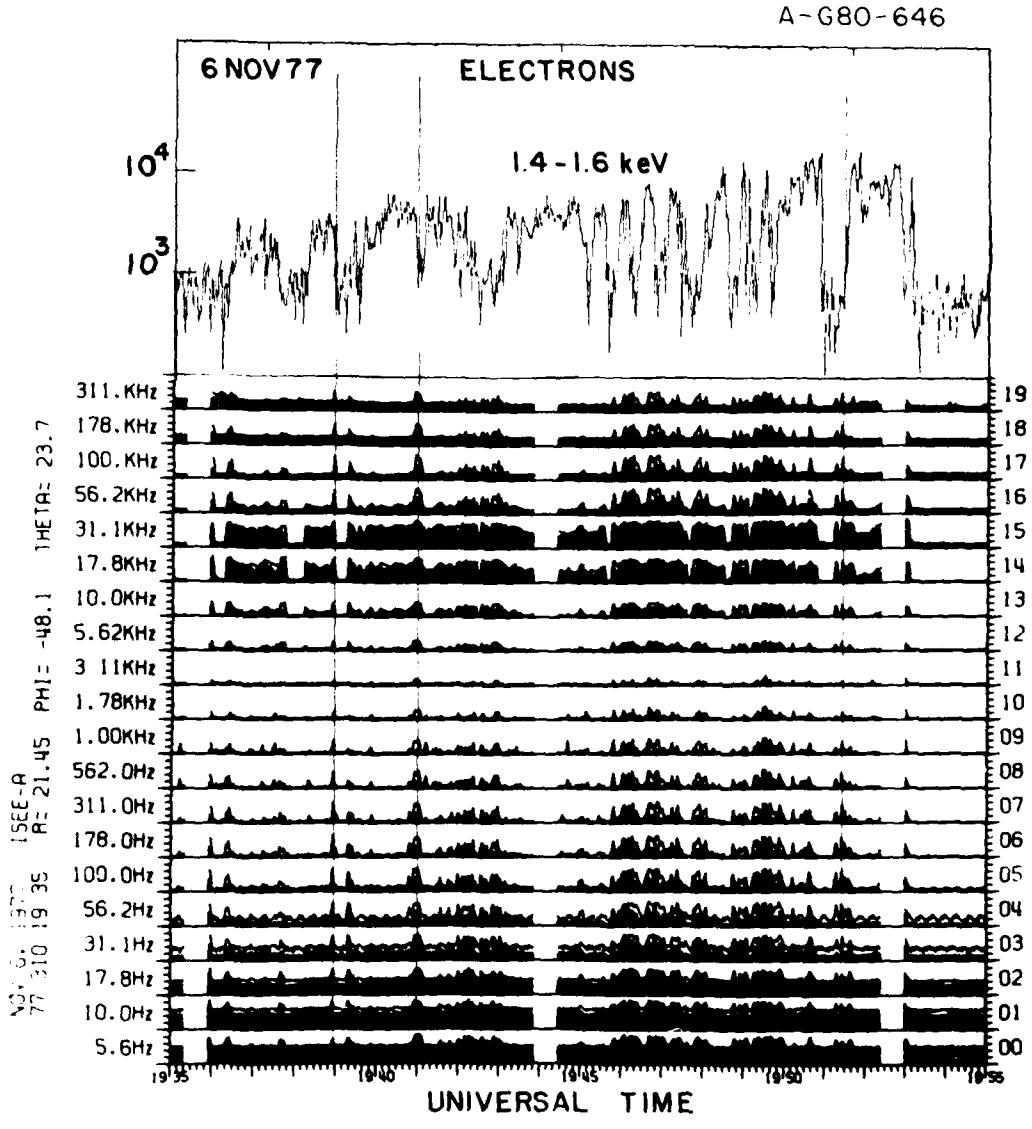
A-G80-646
6 NOV 77
ELECTRONS
1.4 - 1.6 keV
10^4
10^3
311.KHz
178.KHz
100.KHz
56.2KHz
31.1KHz
17.8KHz
10.0KHz
5.62KHz
3 11KHz
1.78KHz
1.00KHz
562.0Hz
311.0Hz
178.0Hz
100.0Hz
56.2Hz
31.1Hz
17.8Hz
10.0Hz
5.6Hz
19
18
17
16
15
14
13
12
11
10
09
08
07
06
05
04
03
02
01
00
ISEE-A
R= 21.45 PHI= -48.1 THETA= 23.7
77 310 19 35
1935
1940
1945
1950
1955
UNIVERSAL TIME

Figure 12

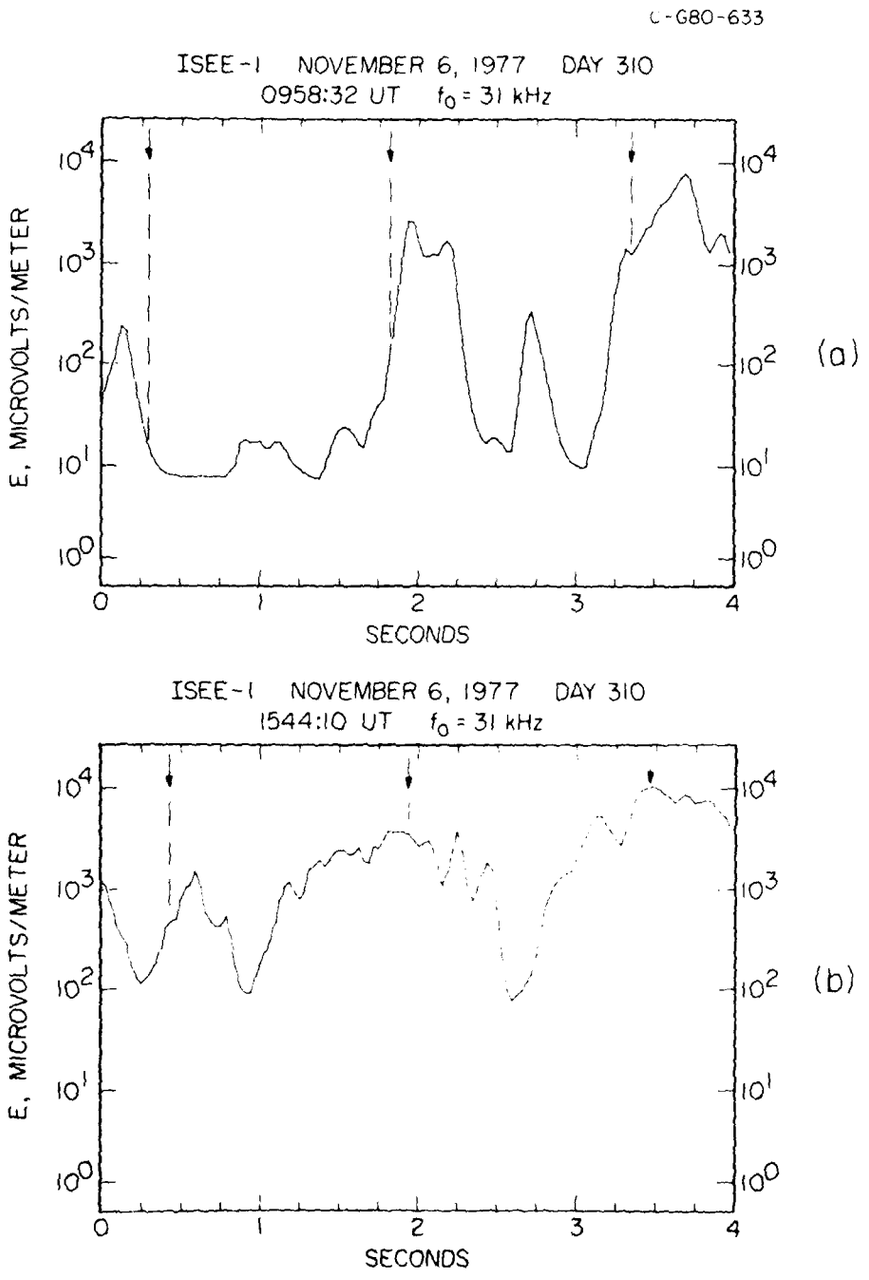
C-G80-633
ISEE-1 NOVEMBER 6, 1977 DAY 310
0958:32 UT f_0 = 31 kHz
E, MICROVOLTS/METER
SECONDS
(a)
ISEE-1 NOVEMBER 6, 1977 DAY 310
1544:10 UT f_0 = 31 kHz
E, MICROVOLTS/METER
SECONDS
(b)

Figure 13

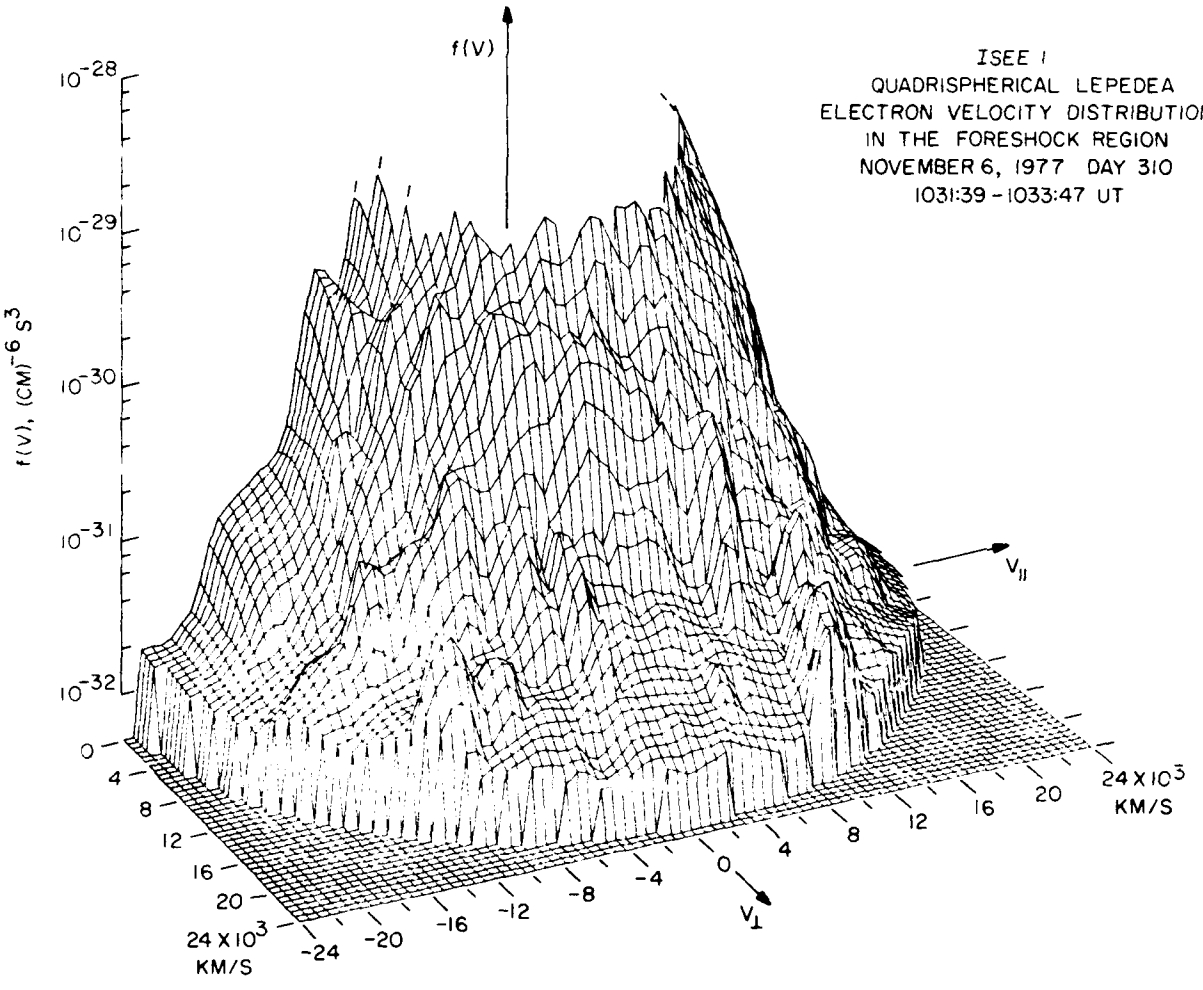
A-G80-665
ISEE I
QUADRISPHERICAL LEPEDEA
ELECTRON VELOCITY DISTRIBUTION
IN THE FORESHOCK REGION
NOVEMBER 6, 1977 DAY 310
1031:39 - 1033:47 UT
f(V)
f(V), (CM)$^{-6}$ S^3
10^{-28}
10^{-29}
10^{-30}
10^{-31}
10^{-32}
$V_{||}$
$V_\perp$
0
4
8
12
16
20
24 X 10^3 KM/S
-24
-20
-16
-12
-8
-4
0
4
8
12
16
20
24 X 10^3 KM/S

Figure 14a

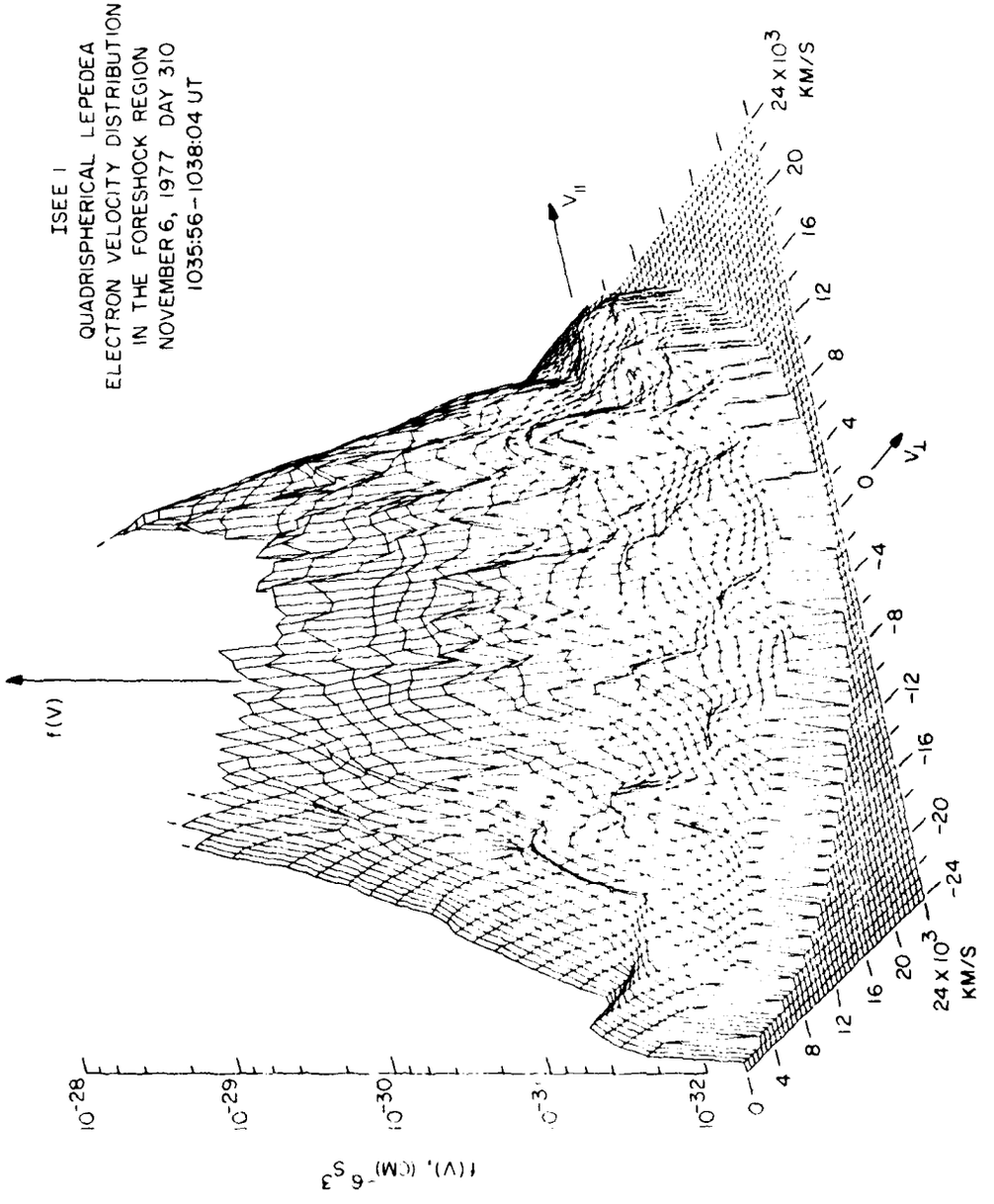
A-G80-666
ISEE 1
QUADRISPHERICAL LEPEDEA
ELECTRON VELOCITY DISTRIBUTION
IN THE FORESHOCK REGION
NOVEMBER 6, 1977 DAY 310
1035:56-1038:04 UT
f(V)
$V_{\parallel}$
$V_{\perp}$
24×10^3 KM/S
24×10^3 KM/S
$f(V), (CM)^{-6} S^3$
10^{-28}
10^{-29}
10^{-30}
10^{-32}

Figure 14b

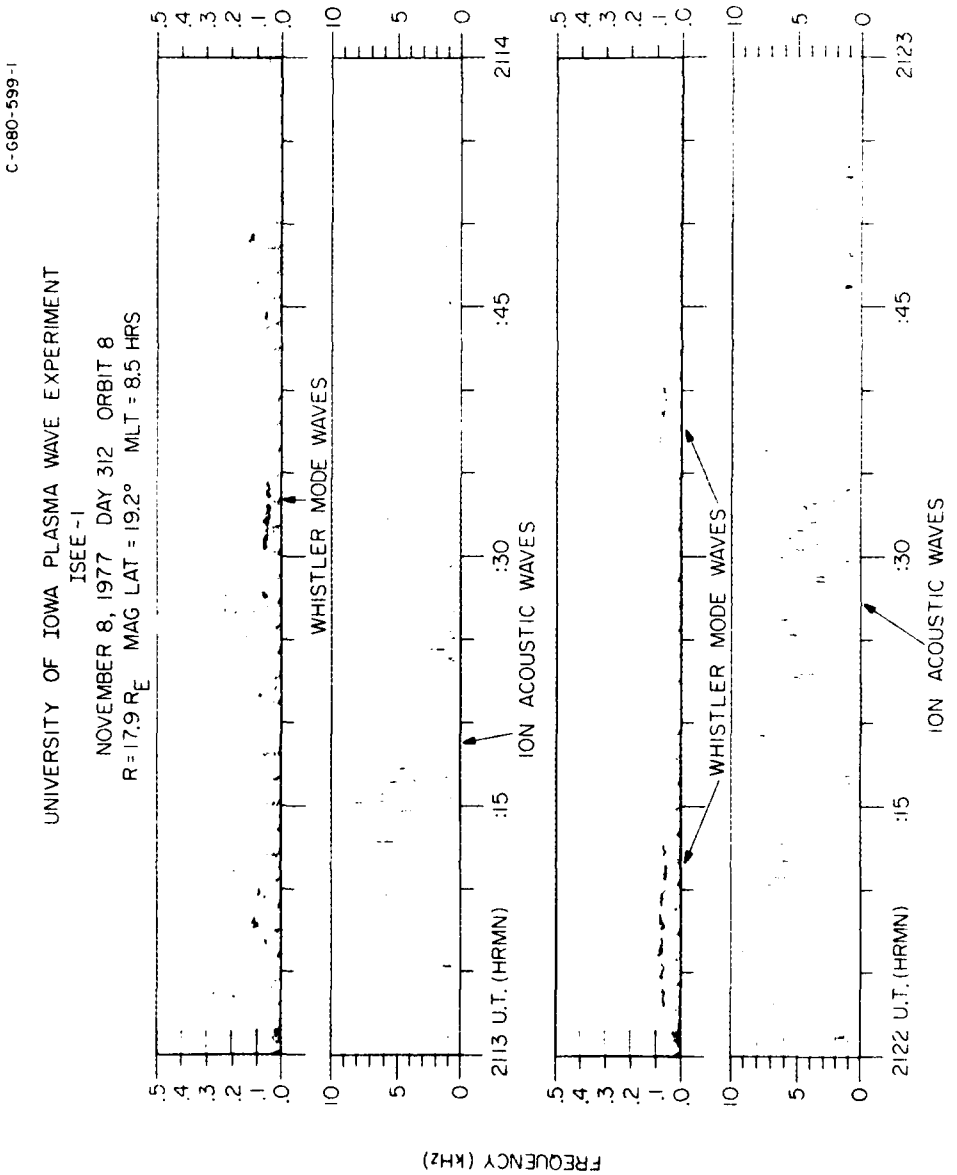
C-GBO-599-1
UNIVERSITY OF IOWA PLASMA WAVE EXPERIMENT
ISEE-1
NOVEMBER 8, 1977 DAY 312 ORBIT 8
R = 17.9 R_E MAG LAT = 19.2° MLT = 8.5 HRS
WHISTLER MODE WAVES
ION ACOUSTIC WAVES
WHISTLER MODE WAVES
ION ACOUSTIC WAVES
FREQUENCY (kHz)
2113 U.T. (HRMN)
:15
:30
:45
2114
2122 U.T. (HRMN)
:15
:30
:45
2123

Figure 15

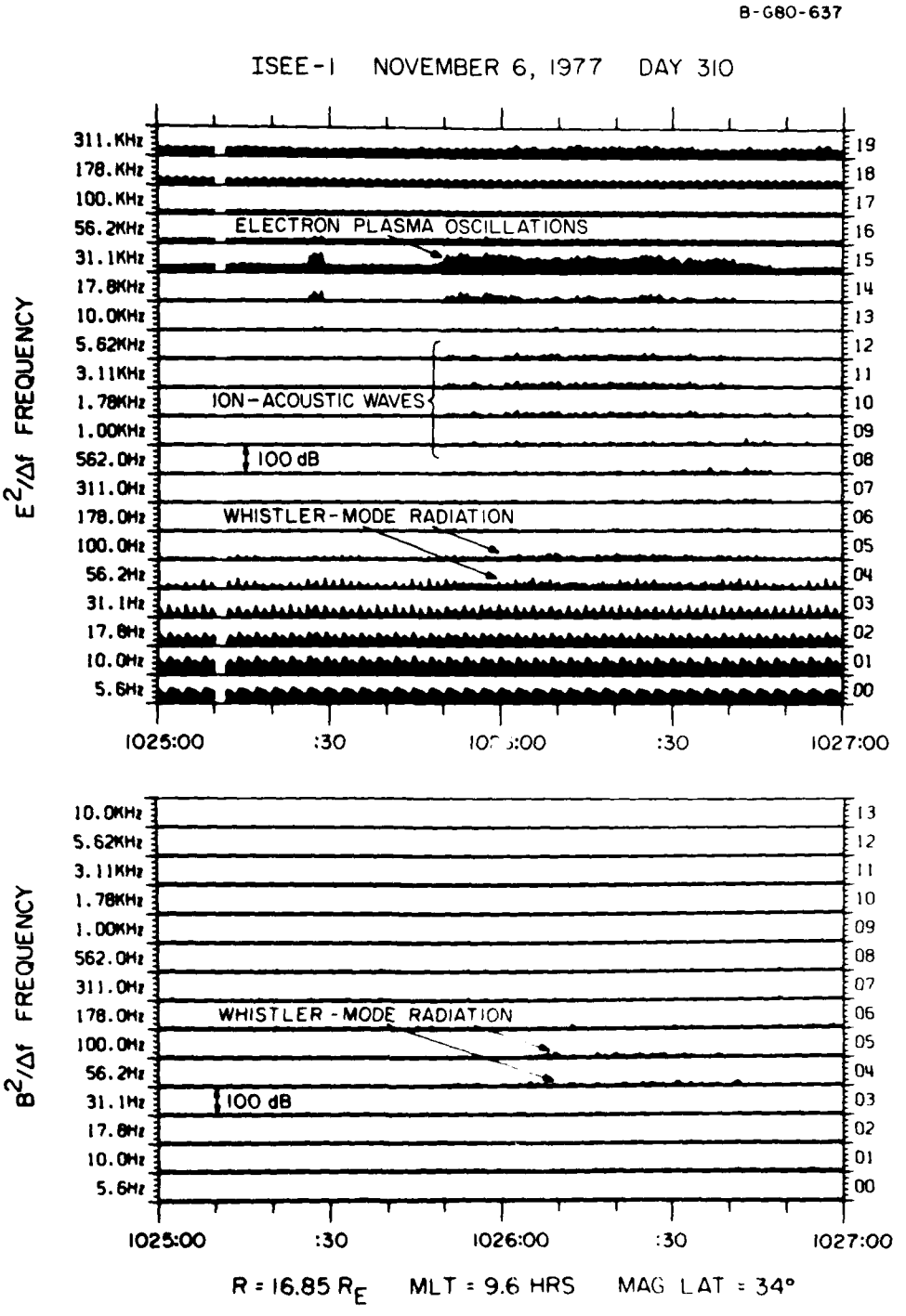
B-G80-637
ISEE-1 NOVEMBER 6, 1977 DAY 310
311.KHz
178.KHz
100.KHz
56.2KHz
31.1KHz
17.8KHz
10.0KHz
5.62KHz
3.11KHz
1.78KHz
1.00KHz
562.0Hz
311.0Hz
178.0Hz
100.0Hz
56.2Hz
31.1Hz
17.8Hz
10.0Hz
5.6Hz
ELECTRON PLASMA OSCILLATIONS
ION-ACOUSTIC WAVES
100 dB
WHISTLER-MODE RADIATION
E²/Δf FREQUENCY
19
18
17
16
15
14
13
12
11
10
09
08
07
06
05
04
03
02
01
00
1025:00
:30
1026:00
:30
1027:00
10.0KHz
5.62KHz
3.11KHz
1.78KHz
1.00KHz
562.0Hz
311.0Hz
178.0Hz
100.0Hz
56.2Hz
31.1Hz
17.8Hz
10.0Hz
5.6Hz
WHISTLER-MODE RADIATION
100 dB
B²/Δf FREQUENCY
13
12
11
10
09
08
07
06
05
04
03
02
01
00
1025:00
:30
1026:00
:30
1027:00
R = 16.85 R_E MLT = 9.6 HRS MAG LAT = 34°

Figure 16

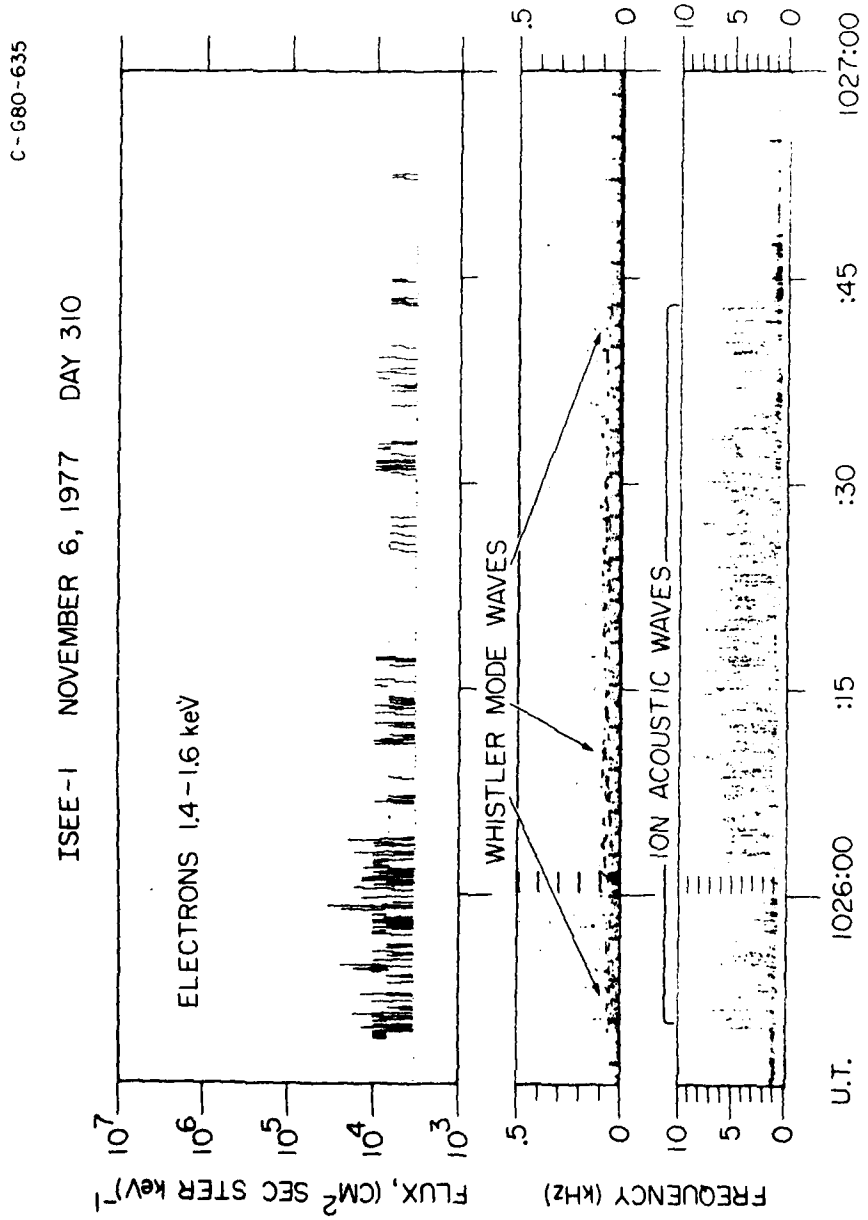
C-680-635
ISEE-1 NOVEMBER 6, 1977 DAY 310
ELECTRONS 1.4-1.6 keV
WHISTLER MODE WAVES
ION ACOUSTIC WAVES
FLUX, (CM² SEC STER keV)⁻¹
FREQUENCY (kHz)
U.T.
1026:00
:15
:30
:45
1027:00

Figure 17

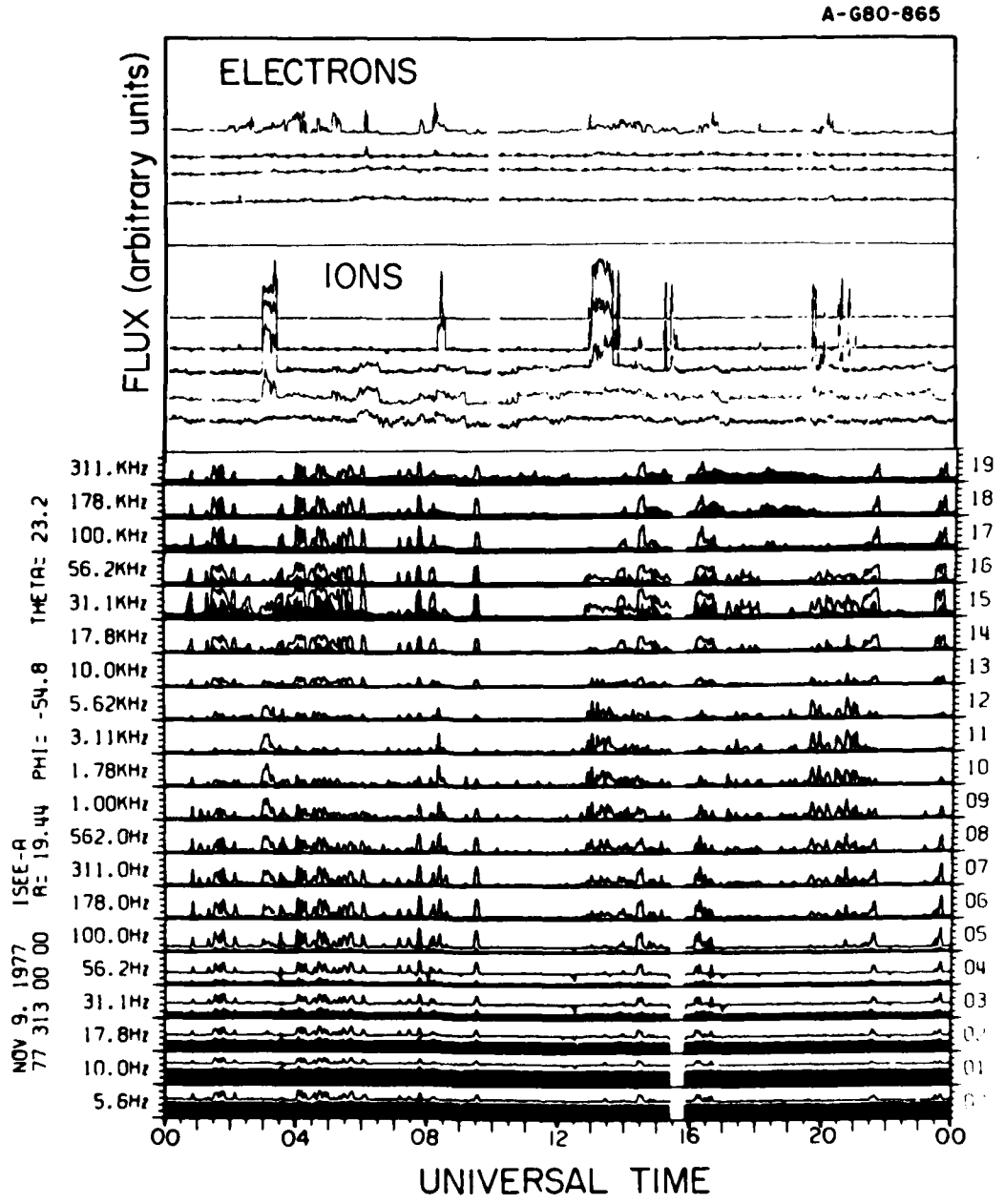
A-G80-865
ELECTRONS
IONS
FLUX (arbitrary units)
311.KHz
178.KHz
100.KHz
56.2KHz
31.1KHz
17.8KHz
10.0KHz
5.62KHz
3.11KHz
1.78KHz
1.00KHz
562.0Hz
311.0Hz
178.0Hz
100.0Hz
56.2Hz
31.1Hz
17.8Hz
10.0Hz
5.6Hz
19
18
17
16
15
14
13
12
11
10
09
08
07
06
05
04
03
01
NOV 9, 1977 ISEE-A
77 313 00 00 R= 19.44 PHI= -54.8 THETA= 23.2
00
04
08
12
16
20
00
UNIVERSAL TIME

Figure 18

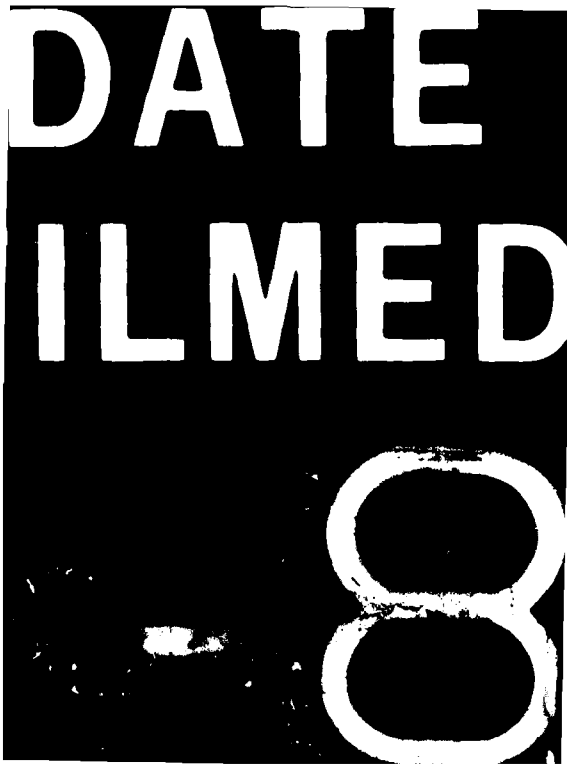
DATE
ILMED
8